Powder Technology 434 (2024) 119356

Contents lists available at ScienceDirect

Powder Technology

journal homepage: www.journals.elsevier.com/powder-technology

Laser powder bed fusion recoater selection guide—Comparison of resulting powder bed properties and part quality

Max Horn [a,b,*,1], Matthias Schmitt [a,b,1], Lukas Langer [a,c], Georg Schlick [a], Christian Seidel [a,d]

[a] Fraunhofer Institute for Casting, Composite and Processing Technology, Am Technologiezentrum 10, 86159 Augsburg, Germany
[b] Technical University of Munich, Institute for Machine Tools and Industrial Management, Boltzmannstrasse 15, 85748, Garching n. Munich, Germany
[c] University of Augsburg, Chair of Digital Manufacturing, Am Technologiezentrum 8, 86159 Augsburg, Germany
[d] Munich University of Applied Sciences, Smart Manufacturing Lab, Lothstrasse 34, 80335 Munich, Germany

HIGHLIGHTS

- Hard recoaters achieve higher accuracies in steady-state processes.
- Soft recoaters are better suited for parameter development and design studies.
- Particles abraded from hard recoaters are more critical than soft recoater erosion.
- Transferability between recoaters can be ensured to a large extent.
- Recoaters can be chosen based on the processing aim and the application.

GRAPHICAL ABSTRACT

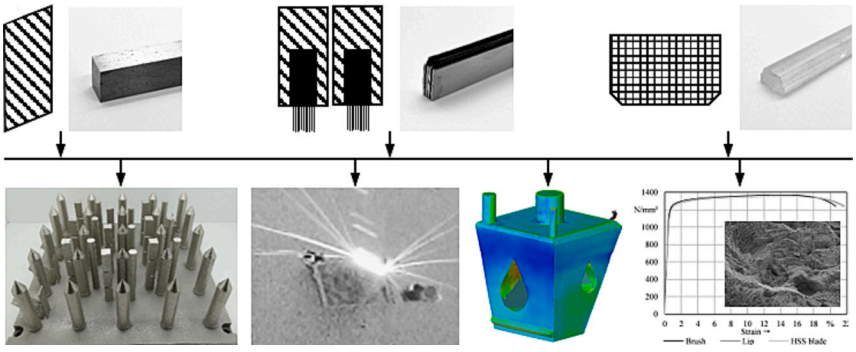

ARTICLE INFO

Keywords:
Additive manufacturing
Laser beam melting
Powder bed fusion, PBF-LB/M
Recoater
Spreading device
Benchmark

ABSTRACT

Spreading devices used to create powder layers in the laser powder bed fusion of metals (PBF-LB/M) were found to have a significant impact on the additive manufacturing process. However, previous research primarily focused on theoretical investigations, including recoater concepts that are not available on the market, while no comprehensive comparison of commercially available spreading devices currently exists. The aim of this study is therefore to examine the powder bed properties and part qualities that can be achieved with the three most common types of recoater: carbon fiber brushes, polymer lips, and high speed steel (HSS) blades. Identical build jobs were produced using each of the spreading devices. Their capabilities were assessed by nine evaluation criteria, including dimensional, metallurgical, and mechanical properties and criticality of particles abraded from the spreading devices. Based on these quantitative findings, a spreading device selection guide was compiled for the benefit of PBF-LB/M practitioners. All recoaters yielded processes with high stability and part properties that were on a par with or even outperformed the nominal values from the literature. However, the HSS blade was found to provide higher accuracy and stability in steady-state processes. In turn, the brush and lip are better suited for parameter development and design studies. Additionally, the lip was found to have economic benefits over the brush, while the brush was deemed an effective all-rounder.

* Corresponding author at: Fraunhofer Institute for Casting, Composite and Processing Technology, Am Technologiezentrum 10, 86159 Augsburg, Germany.
E-mail address: max.horn@igcv.fraunhofer.de (M. Horn).
[1] These authors contributed equally to the paper.

https://doi.org/10.1016/j.powtec.2023.119356
Received 16 June 2023; Received in revised form 1 October 2023; Accepted 31 December 2023
Available online 5 January 2024

1. Introduction

1.1. Literature review

The inherent process characteristics of additive manufacturing (AM) make it increasingly suitable for the fabrication of complex parts that serve both functional integration and the tailoring of material and part properties. Benefits such as increased freedom of design, fewer part numbers, and shorter lead times make AM technologies an overall game changer in such industries as aerospace and power generation [1]. By employing powder bed fusion of metals using a laser beam (PBF-LB/M), these first-mover industries are able to produce fully dense components with material properties comparable to those of conventionally manufactured parts [2]. However, the PBF-LB/M process is affected by a great number of parameters and possible disturbances [3,4]. Therefore, quality assurance remains a major challenge in the industrial application of AM technologies [5]. In the case of PBF-LB/M, the in-process performance of metal powders [6]—primarily described by their spreadability—was shown to have a significant impact on part quality [7]. Primary powder properties and the resulting powder bulk behavior, which ultimately contribute to the powder's spreadability have been extensively investigated; Vock et al. [7] provide a comprehensive overview. However, impacts stemming from the AM machine itself—first and foremost the spreading medium used for the metal powders—have been examined less frequently [8].

In accordance with DIN EN ISO/ASTM 52911–1, PBF-LB/M machines use a powder layering system with a spreading device that distributes the feedstock throughout the build surface in even layers [9]. Other technical guidelines and specs refer to the spreading device itself or the entire layering system as a coater [6] or recoater [10,11]. As the latter usage has become widespread, the terms recoater and spreading device will be used synonymously throughout this study. Further synonyms found in the literature include rake [12], spreading tool [8], and wiper [13]. Non-rotating or fixed spreading devices can be divided into hard recoaters, such as high speed steel (HSS) or ceramic blades, and soft recoaters, such as rubber or silicone lips as well as various types of brushes [9]. Although, frequently discussed in academia, rollers [14–18] and contact-free powder layering systems [19] currently play a minor role in commercially available PBF-LB/M machines. Only two manufacturers currently consider such spreading approaches, with the majority of suppliers offering fixed recoating systems. Khorasani et al. give an overview of commercially available PBF-LB/M systems and options [20]. Generally, hard spreading devices are said to apply larger frictional forces to the powder bed than soft devices [9]. Sehhat and Mahdianikhotbesara [8] conducted a literature review on powder spreading in PBF-LB/M. The researchers concluded that a device's spreading performance is a function of its *motion*, *geometry*, and *material*. We therefore present the academic findings regarding the impact of spreading devices on powder spreadability for these three parameters.

The influence of a spreading device's *motion* of on powder bed density and surface roughness has primarily been investigated for rollers [14–17]. Although the roller concept was found to have a certain advantage over fixed spreading devices for thin powder layers [21], PBF-LB/M machines are dominated by the latter – primarily blades, lips, and brushes. Xiang et al. [22] used simulation methods to show that powder spreadability is highly correlated to the velocity of the spreading device. Using a similar approach, Meier et al. [23] contributed to the discussion of whether increasing the spreading velocity of a rigid blade leads to decreased layer quality. Mitterlehner et al. compared the powder bed densities (PBD) obtained with a rhombic HSS blade when applying different recoating strategies and showed that wiping off excessive powder when the blade moves back over the powder bed leads to compaction, which significantly increases the PBD [24,25]. Spreading velocities of >200 mm/s were not recommended, as they lead to the formation of irregular surface defects. In contrast, Snow et al. found that higher recoater velocities led to increased powder spreadability [26].

Wang et al. [27] used the discrete element method (DEM) to investigate powder spreading behavior based on different *recoater geometries,* including vertical, angled, and round blades as well as rollers. The majority of homogeneous layers were formed with a rotating roller. Round and inclined blades compacted the powder in front of the recoater during spreading, leading to an increase in PBD. In contrast, higher forces were transferred to the underlying parts when using blades. These findings are in line with the further investigations conducted by Cao [28] and Le et al. [29]. Both found that recoater geometries that apply forces to the powder using a planar surface rather than a point create higher-quality powder beds. Hence, sharp edges, such as those found on blades, tend to jam particles, resulting in lower-quality powder layers. Haeri [30] added to the discussion that fixed blades can lead to better powder spreading results by applying an optimized blade geometry. The novel geometry facilitated the formation of a super-elliptic edge profile and outperformed a roller in terms of PBD and layer surface roughness.

Diegel and Wohlers described possible spreading device *materials,* and concluded that hard recoaters apply more pressure to the powder bed, which renders them prone to process failure if they come into contact with protruding parts [13]. Daňa et al. [31] investigated the use of a rigid ceramic blade as a recoater and came to a similar conclusion. The rigidity characteristic was less suitable for protruding parts and support structures. For complex parts, a flexible recoater was recommended, albeit without any detailed description of such a medium. In addition to the spreading device's stiffness and hardness, its surface was also found to play a significant role. Chen et al. [12] found that the powder packing density can be increased by lowering the friction coefficient of spreading devices, for instance, by surface modification. Moreover, powder layer surface properties were improved by Meier et al. [23], using a recoater with low adhesive interaction with the feedstock. These findings match the findings of Snow et al. [26]. Generally, powder particles tend to stick to the spreading device as its friction coefficient increases, which negatively influences the powder layer quality [32].

In contrast, there is very little research that associates the given findings with in-process spreading performance and resulting part properties. In a review paper on support-free PBF-LB/M processes, Weber et al. [19] concluded that the use of a recoater can significantly increase the need for support structures. Contact-free recoating is considered a particularly promising way of removing the need for support structures. However, the resulting powder bed density and part quality are not considered. Shamsdini et al. [33] investigated the tensile properties of maraging steel specimens manufactured by PBF-LB/M using a ceramic blade and a carbon fiber brush. They stated that the hard recoater blade applies pressure in the recoating direction, leading to a denser powder bed, whereas the brush spreads the powder more gently, without applying any pressure. The experimental results indicated that neither the ultimate tensile strength (UTS) nor the yield strength (YS) are affected, while the ductility of the samples manufactured with the brush recoater is reduced. Fracture surfaces revealed unmelted powder in one specimen manufactured with the brush. Although the PBD was measured, no clear correlation or explanation was presented. Ali et al. [34] went into greater detail by investigating the powder bed of Hastelloy® X on an EOS M290 machine. They found that the PBD fell from 66 to 52% in the recoater direction. The segregation of particles along the spreading direction of a rigid recoater was given as a possible explanation. The reduced PBD led to a 0.25% decrease in part density along with increased surface roughness. Apart from the difference in the forces applied to the powder bed, soft recoaters are often said to be more prone to wear and that any particles abraded from the spreading devices can have a negative impact on part properties. In this context, Palm et al. [35] investigated the influence of recoater brush hair and other contaminants on part quality. They found that the fibers did not affect either the part density or its microstructure. However, there have been no studies examining their impact on mechanical properties.

Even less information is available that might help PBF-LB/M operators to choose the most suitable spreading device for their application. Guidelines for recoater selection are given by PBF-LB/M machine manufacturers like EOS. These state that soft recoaters—particularly brushes—should be used for manufacturing parts with high aspect ratios [36]. In contrast, hard recoating is preferred in safety-critical industries and for maximum part quality. This advice is, however, not underpinned by empirical data, and no correlations to powder and part properties are disclosed. Furthermore, the literature review showed that only straight-line recoaters, perpendicular to the spreading direction, are currently in use. The use of angled spreading devices could imply certain advantages, for example, in terms of powder consumption. However, this aspect is not covered in the present study.

1.2. Problem statement and approach

It can be concluded that the majority of studies follow an inductive approach and address the fundamental relations between spreading device motion and geometry, as well as material and powder spreadability. However, findings regarding spreading device *motion* are inconclusive for fixed hard recoaters, while there are none at all for soft recoaters. Thus, no conjecture to be tested was derived. Simulative approaches identified recoater *geometries* that reduce the unsuitable forces applied to the powder bed. The variety of geometries actually available for PBF-LB/M has, however, not been taken into consideration. Yet, two conjectures were derived from the literature, applicable to commercially available spreading devices: Sharp edges on hard recoaters can jam particles, which leads to streaks and a segregation of particles in the powder bed along the recoating direction (1). Furthermore, recoaters with planar surfaces create higher-quality powder beds than recoaters having sharp edges (2). In terms of the *material*, hard recoaters like HSS or ceramics and their respective geometries have been well investigated through simulation, although soft recoaters are not evaluated in simulation models. While recoater materials with low friction coefficients are preferable in terms of spreadability and lip availability, brushes and blades apply entirely different forces to the powder bed, and their friction coefficients are scarcely comparable. The majority of studies agrees that hard recoaters apply higher forces to the powder bed, yield higher powder bed densities, and therefore transfer higher forces to the underlying parts (3). Furthermore, hard recoaters are more prone to process failure (4). Additionally, soft recoaters are more prone to wear and abraded particles have a negative influence on part quality (5).

These fundamental findings have not yet been fully linked to the resulting powder bed and part properties. Even though part designers and PBF-LB/M machine operators need to consider the impact of recoater types on process results, no independent selection guide for spreading devices currently exists that is substantiated by empirical data.

Against this background, this deductive study investigates the influence of commercially available recoater types that are in widespread use, to determine their impact on powder properties and part quality. The five major conjectures (1–5) from the literature, as summarized above, should be tested in an industry-relevant context. Three types of spreading devices were selected for the study, based both on their availability and distribution and, in turn, their relevance to PBF-LB/M. These are a pure carbon brush (denoted here as ***brush***), a polymer lip made of silicon (denoted as ***lip***), and a high speed steel blade (denoted as ***HSS blade***). Build jobs were designed and performed that enabled evaluation of the resulting powder and part properties, based on the following criteria:

- Powder properties:
  - o Powder bed surface uniformity
  - o Powder bed density
  - o Particle size distribution
- Part properties:
  - o Buildability
  - o Surface roughness
  - o Dimensional accuracy
  - o Density and metallurgical structure
  - o Tensile strength
  - o Criticality of particles abraded from the spreading devices

The build jobs were fixed and repeated on a single machine using a single material system for each of the selected spreading devices, as described in the following section. Findings and process fundamentals were used to discuss conjectures from the literature. Finally, all results were subjected to a pairwise comparison for each criterion and each spreading device, in line with VDI 2225 [37], and a selection guide was compiled that can be used by PBF-LB/M operators.

2. Materials and methods

2.1. Sample manufacturing

The specimens were manufactured on an EOS M290 mid-size industrial PBF-LB/M machine (Electro Optical Systems GmbH, Krailling, Germany). It is one of the most widely used PBF-LB/M systems, and its results should thus be directly transferable to a large group of users and other PBF-LB/M machines operating with similar recoaters. The machine's uniaxial coating system limits the number of influence factors, which makes it well suited to this study.

Ni-base alloy 2.4668 (NiCr19Fe19Nb5Mo3 or Inconel® 718) metal powder with a nominal particle size distribution (PSD) of 15–45 µm supplied by Praxair Surface Technologies (Indianapolis, IN, USA) was used for all build jobs. The material was chosen for its level of distribution as well for its relevance to aerospace, which is not only a pioneering industry for PBF-LB/M but also a leading sector for this manufacturing technology [38]. Hosseini and Popovich give a general overview of the material and properties that can be achieved with PBF-LB/M [39]. The powder used in this investigation was gas atomized under argon atmosphere. Fig. 1 shows the PSD along with a scanning electron microscope (SEM) image of the actual powder used for the underlying investigation. The PSD was slightly narrower than the nominal specification, due to the lower percentage of fine particles. The particles were primarily spherical, with a small number of satellites.

For sample manufacturing, laser parameters from the machine manufacturer were used, with an infill energy density of 67.47 J/mm^3 at a layer height of 40 µm. After the infill, two contour scans were performed. The scan strategy consisted of 10 mm stripes with a rotation of 67° after each layer. There was no fine tuning for dimensional accuracy nor any adjustment of the contour border offsets. All build jobs were conducted on steel baseplates, with a preheating temperature of 80 °C. Argon was used as a shielding gas in all jobs. Powder recoating was performed at a speed of 150 mm/s, which is within the range suggested by Snow et al. [26]. The manufacturing parameters and boundary conditions of all specimens were fixed, while the build preparations were performed by a single operator according to the manufacturer's guidelines. Only the powder spreading device was changed for each job. For this study, hard recoating was performed with an HSS blade, while a brush with two rows of pure carbon fiber and a polymer lip, made of silicon, were used as soft recoaters. Fig. 2a shows a schematic of each type of spreading device. A virgin spreading device was used for each of the build jobs. All three recoaters are available commercially and were procured from EOS GmbH (Krailling, Germany), the manufacturer of the PBF-LB/M machine. Following each build job, all the powder was removed from the machine, the build chamber was cleaned by vacuuming, and the powder was sieved at a mesh size of 63 µm, after which the machine was set up for the next build job. The specimens were manufactured by re-using the same powder in each subsequent build job, with no further intermediate use of the machine.

To investigate the influence of various powder spreading devices on

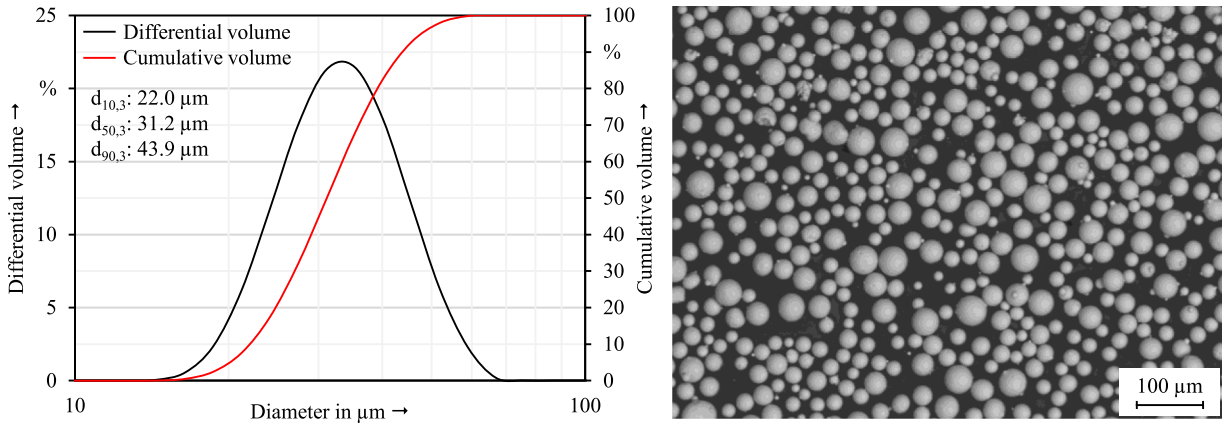

Fig. 1. Semi logarithmic graph of the volumetric particle size distribution (left), and a scanning electron microscope image (right) of the 2.4668 metal powder used for this investigation.

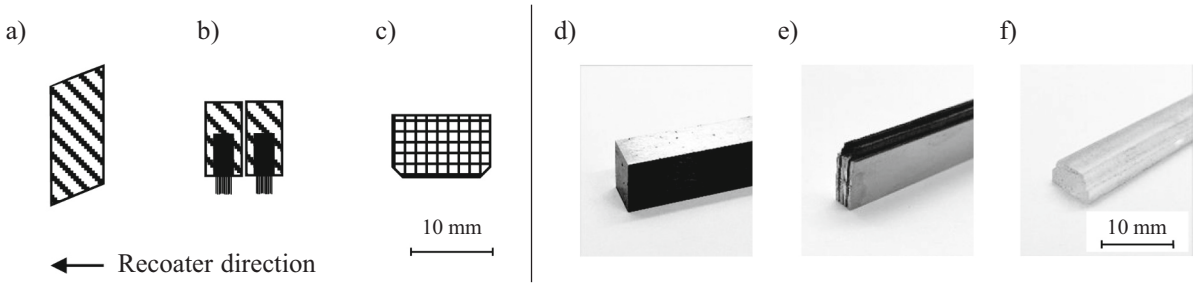

Fig. 2. Schematic cross-sections of the spreading device geometries a) HSS blade, b) carbon fiber brush, and c) polymer lip (NB: clamping devices not shown) as well as images of the actual spreading devices d) HSS blade, e) carbon fiber brush, and f) polymer lip.

the PBF-LB/M process and the resulting part properties, five different test piece geometries were manufactured (Figs. 3 and 4). Cylindrical specimens with tapered tips were used to analyze the powder bed properties. The insides of the specimens were hollow and served as a powder store to enable analysis of the powder after each build job. For mechanical analyses, cylindrical specimens with a diameter of 9 mm were built and machined to form tensile specimens according to DIN 50125. For each variant, at least seven specimens were tensile tested. Blocks with the dimensions 10 × 10 × 75 mm^3 were used for density measurements and microstructure analysis. These were divided into three areas (bottom, middle, and top) by the surrounding edges. Fig. 3 shows the dimensions of all the specimens. To determine the influence of the recoater on the general buildability of thin structures, walls were built at 90° and 45° angles to the build plate, with a length of 25 mm, a height of 40 mm, and various thicknesses (0.2, 0.4, 0.6, and 0.8 mm). The walls with a 45° angle were tilted in the direction of the recoater movement. A complex specimen (Fig. 4) consisting of a variety of overhang surfaces, pins, and boreholes was designed to obtain information regarding any possible dependency between the dimensional accuracy and the recoaters and to evaluate the overall accuracy.

First, three identical jobs were built using three different spreading devices. These included powder, tensile and microstructure specimens (build jobs one to three). Thin walls and a test artefact were placed between the specimens. The full layout is shown in Fig. 5 (left). The powder specimens were evenly distributed in a 5 × 5 pattern to enable local evaluation of the powder properties on the build plate including the gas flow and recoater directions. The tensile and microstructure specimens were distributed in the middle of the build plate in a 3 × 3 pattern.

A further build job was created to investigate the influence of potential contamination through abrasion of the recoater from interaction with protruding edges or parts (build job four). In total, the fourth build

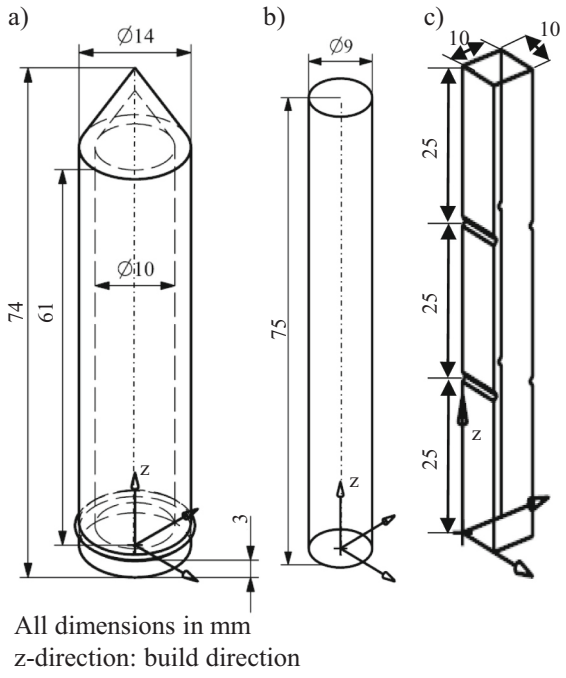

Fig. 3. a) Powder specimen, b) tensile specimen with machining allowance, and c) microstructure and dimensional specimen.

job consisted of 28 tensile specimens and four specimens for computer tomography (CT) investigation. The layout of this build job is shown in Fig. 5 (right). The contaminants were extracted from each recoater by

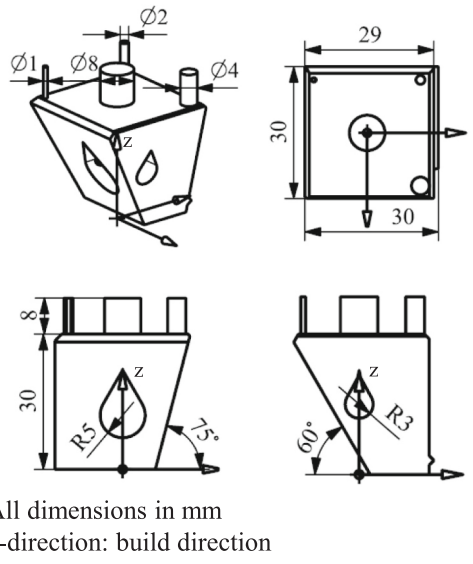

Fig. 4. Geometry specimen with overhangs, pins and drop-shaped cutouts in various sizes.

various methods. Individual hairs of an approximate length of 0.5–1 mm were cut from the carbon brush using pliers. The polymer lip was cut and shredded into small irregular particles with lengths of approximately 0.5 mm. Chips of around 250 µm in size were taken from the HSS blade using a cutting tool. Fig. 6 shows SEM images of the contaminants, with the irregular shapes and sizes clearly visible.

The build job was interrupted at a 50% build height after powder recoating. The build chamber was opened and the powder layer on top of seven tensile specimens and one CT specimen were contaminated with abrasions from each of the spreading devices. A further seven tensile specimens and one CT specimen were not contaminated and acted as reference samples. After placing each of the contaminants on the respective powder bed, the chamber was closed, process conditions re-established, and solidification of the layer resumed. The entire interruption related to the contamination procedure lasted 33 min and 42 s from the final recoating step until exposure of the contaminated powder layer. The build platform heater remained active during the interruption.

After each build job and—where necessary—following initial analyses of the build plate, all parts were removed from the plates using wire electrical discharge machining (EDM). All tensile and microstructure specimens were then heat treated in a vacuum furnace (SECO/WARWICK S.A., Swiebodzin, Poland) under vacuum (≤ 0.000016 mbar), as suggested by the Association of German Engineers (VDI) [40] in accordance with SAE AMS5662N, as follows [41]:

- Solution annealing: 1 h at 980 °C, air cooling to room temperature
- First artificial ageing: 8 h at 720 °C, furnace cooling (16 K/min) to 620 °C
- Second artificial ageing: 10 h at 620 °C, air cooling to room temperature

2.2. Powder analysis

Immediately following build jobs one, two, and three, images of the top layer of the powder bed were obtained for qualitative comparison using a compact camera (Canon Inc., Ōta, Tokyo, Japan). The PBDs throughout the build platform were analyzed using a method inspired by previous research [34,42–44]. The 25 powder containers (Fig. 3a) from each build job were weighed using a Kern PLJ 360-3NM precision scale (KERN & SOHN GmbH, Balingen-Frommern, Germany). The PBD was

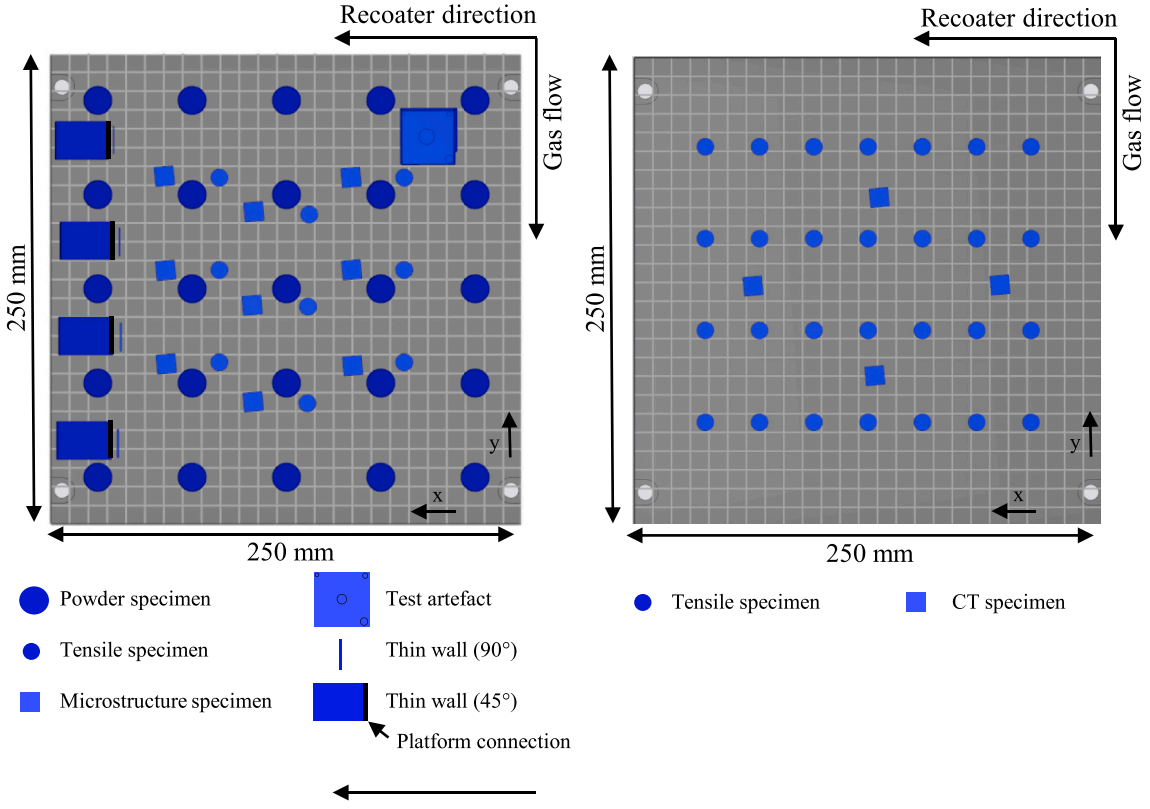

Fig. 5. Layout of build jobs one, two, and three used for comparing the spreading devices (left) and build job four used to investigate the influence of contamination from the recoaters (right).

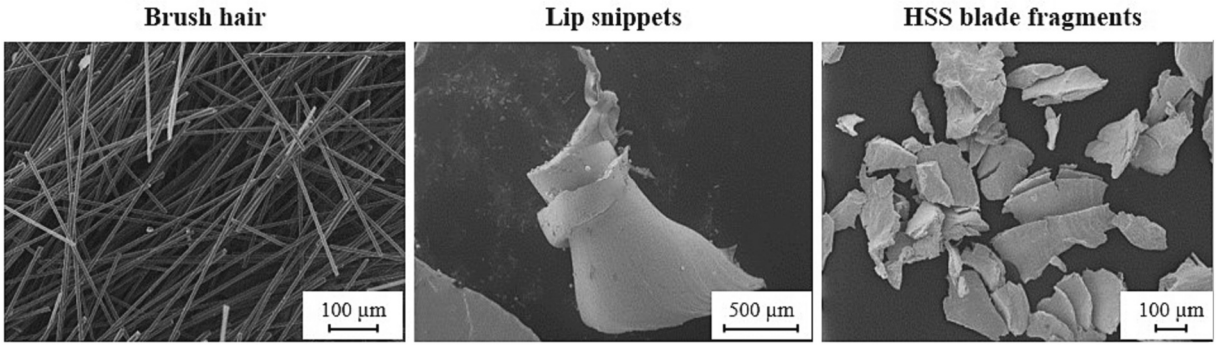

Fig. 6. Scanning electron microscope (SEM) images of contaminations.

then calculated by subtracting the mass of the solidified outer shell of the powder container from the total weight and dividing the result by the volume of the non-solidified space inside the container. The mass of the outer shell was estimated based on a volume of 5.2415 cm^3 as obtained from the CAD software, a material density of 8.20 g/cm^3 [45], and a porosity of 0.1%. According to the CAD software, the volume of the non-solidified space where the powder was collected during the build job was 4.7820 cm^3. Height variations of the powder containers due to having been cut from the build plate were checked using a caliper gauge and incorporated accordingly in the calculation.

The powder specimens were then cut open manually at the top, after which the powder was released, sieved to extract shavings, and collected. The PSD of the collected powder was then analyzed by laser diffraction, employing wet dispersion and ultrasound using a Mastersizer 3000 device (Malvern Panalytical Ltd., Malvern, UK). Each of the 25 powder containers from each build job was split into three samples, and five measurements were conducted on each of them.

2.3. Part analysis

2.3.1. Buildability

The buildability of the thin wall specimens was rated to enable evaluation of the impact of the spreading devices on the buildability of geometrically complex features such as lattices or parts with high aspect ratios. Following an optical inspection, the walls were rated either as "successfully built" or "failed". A failed rating was given when either an incomplete build, strong bending, delamination, or a lack of layer adhesion was observed. The evaluation was also applied to determine the suitability of a recoater for the development of new material parameters or for the specific tuning of laser parameters, as part protrusions or elevated melt pools can also cause contact with the recoater.

2.3.2. Surface roughness

Surface roughness was measured optically using a Keyence VK9700 laser scanning microscope (LSM) (Keyence Corporation, Ōsaka, Japan). At least five measurements of ~4.94 mm^2 each were taken with a magnification of 10× and not further filters on the vertical side of the microstructure specimens and mean values of the arithmetical mean (Sa) and the maximum height (Sz) of the area were derived in accordance with ISO 25178 [46].

2.3.3. Dimensional accuracy

The dimensional accuracy of rectangular geometries on the microstructure specimens (Fig. 3c) was determined prior to heat-treatment in as-built condition using a digital caliper (Mitutoyo Corporation, Kawasaki, Japan) with a maximum permissible error (MPE) of 20 µm in accordance with ISO 10360 [47]. All nine specimens from each spreading device were measured five times at the top, middle and bottom and the mean values calculated.

The overall dimensional accuracy of each spreading device was evaluated by blue light inspection of the geometry specimens (Fig. 4). The 3D scans were conducted with an Atos Core 300 device (GOM GmbH, Braunschweig, Germany). The blue light inspection was based on fringe patterns from a projector recorded by two cameras and the projector. A 3D point cloud was generated from the three different angles to the part's surface. Geometrical accuracy and deviations were evaluated by aligning the 3D point cloud (after polygonization) with the CAD data using GOM Inspect 2019 software (GOM GmbH, Braunschweig, Germany).

2.3.4. Density and microstructure

The absolute density was measured by applying the Archimedean principle in air and 2-propanol at room temperature. All microstructure specimens (Fig. 3c) were measured three times using the Kern PLJ 360-3NM precision balance. The microstructures were evaluated by cross-sectioning the specimens parallel to the build plane (x-y-plane) and parallel to the build direction. Following grinding and polishing of the samples on a SAPHIR 530 device (ATM Qness GmbH, Mammelzen, Germany), the relative optical density was measured using a BX53M optical light microscope (OLM) (Olympus Corporation, Shinjuku, Japan). The samples with the highest and the lowest absolute density from each recoater were examined at 5× magnification. To quantify the relative optical density, a total area of ~44 mm^2 was analyzed per spreading device. Microstructure images were taken after twenty seconds of etching with V2A etchant at 60 °C.

2.3.5. Tensile strength

Tensile strength was analyzed after machining and heat treatment of all tensile specimens (Fig. 3b, build jobs one - four) in accordance with DIN EN ISO 6892-1 [48]. All tests were conducted on a Zwick Z050 device (Zwick GmbH & Co. KG, Ulm, Germany) at room temperature. Fracture surfaces were then examined using a TM3030 scanning electron microscope (SEM) from Hitachi Ltd. (Chiyoda, Tokyo, Japan).

2.3.6. Porosity analysis

Porosity analysis using CT scans was only conducted for the microstructure specimens (Fig. 3c), based on the contamination build job (fourth job). Samples with a thickness of 2 mm were cut from the respective CT specimens 1 mm above and 1 mm below the contamination plane. All measurements of the 10 × 10 × 2 mm^3 cuboids were conducted with a v|tome|x m micro CT (Baker Hughes Company, Houston, TX, USA) with a voltage of 300 kV, resulting in a voxel size of 18 µm and a minimum detectable pore size of approximately 36 µm in diameter. The relative density and pore distribution were then evaluated to assess the criticality of the contamination in regard to the reference condition. The aim was to reveal an overall pore distribution of the contaminated area.

3. Results

3.1. Manufacturing report

We begin with a qualitative description of the observations made during and after manufacturing. Fig. 7 shows example images of the powder bed following a build process, along with cleaned specimens on the build plate. One build job was created with the layout shown in Fig. 5 (left) for the brush and lip. The first build job using the HSS blade failed due to contact with the thin wall specimens and was halted after the build height reached approximately 20 mm. An image of the failed specimens is included in Appendix A1. The thin wall specimens were omitted in the subsequent build job with the HSS blade, and a successful build was achieved. The build job with the lip as a recoater medium revealed damage to the lip due to contact with one of the thin walls. However, it only affected some of the layers in three parts, and the overall build job did not fail. The build job with the brush was entirely unobtrusive. Following these three build jobs, the specimens for the contamination tests were made using a brush as the spreading device, due to the robustness observed in the first three jobs.

3.2. Powder properties

3.2.1. Powder bed surface uniformity

A qualitative rating of the powder bed uniformity was conducted after each build job. The powder bed was inspected manually and images obtained, as shown in Fig. 8. The ratings took into consideration agglomerations, grooves, and discontinuities in general. The brush created an almost homogeneous powder bed, with a small streak near the build plate edge probably caused by a brush damaged by protruding thin walls. A similar but more pronounced streak was observed when using the lip as a recoater. In comparison to the lip, the brush appeared able to recover to an extent from contact with protruding parts. The build job with the HSS blade had to be built without thin wall specimens, after the first job failed due to harsh contact with the recoater (see Appendix A1). This is one reason why the powder bed showed a high level of homogeneity and no streaks. All in all, no significant differences in the powder bed areas without streaks were detected in conjunction with the spreading device used.

3.2.2. Powder bed density and particle size distribution

The results of the PBD and PSD analyses are displayed in Fig. 9, in which the numbers represent the values measured at the respective positions on the build plate. Mean values and standard deviations of the job are given below each build plate. An “X” indicates that the measurement was not possible. Three powder containers manufactured using the lip were damaged due to contact with the failed thin walls, while one container made with the brush broke during opening. As a result, the PDB was measured, while some PSD values are missing. In general, the PBD is highly constant within every build job and across the various spreading devices. The blade and brush might indicate a slight decrease in the PBD along the shielding gas flow, but given the non-standardized measuring technique, the differences cannot be seen as statistically significant. Also, no trend in the PBD in relation to the recoating direction was observed for any of the spreading devices. PBD values show little variance both within each job and between the spreading devices.

Similar results are shown for the percentiles of the particle size distributions. A slight trend towards coarser particles can be observed from the top right to the lower left corner of each build job. However, considering the standard deviation of the measuring method indicated by the overall mean values, the significance of this trend is uncertain. Overall, the PBD and the PSD show high levels of homogeneity within each build job and between the spreading devices.

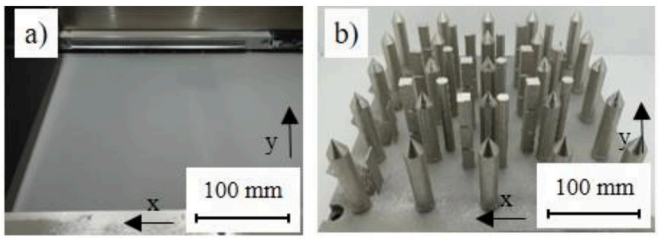

Fig. 7. a) Example image of the powder bed after the build job b) Example image of the specimens on the build plate after cleaning.

3.3. Part quality

3.3.1. Buildability

The first evaluation criterion for spreading devices with regard to part quality is their suitability for manufacturing complex structures. Depending on the material and processing window, the parts might be affected by elevated edges or protrusions, which can cause recoater contact. Depending on the flexibility and material of the recoater, it will either give way, for instance by bending or delamination, or the part will be bent by a rigid recoater material, potentially leading to plastic deformation. Similar effects occur when processing parts with low stiffness, e.g. thin walls with a high aspect ratio. To evaluate buildability, thin walled structures were built and the resulting parts rated. An overview of the ratings is given in Table 1. Regardless of the overhang angle or part thickness, none of the specimens could be built successfully using the HSS blade. The parts showed severe plastic deformation due to recoater contact (bending in recoater direction, see Appendix). Using a brush or lip led to successful thin wall builds with a minimum thickness of 0.6 mm (45 and 90° angles). Specimens with a lower wall thickness failed due to delamination or bending.

3.3.2. Surface roughness

Before analyzing the microstructure, the surface roughness of the specimens was determined by taking five measurements using the middle segment of the dimension specimens. The mean values and standard deviations are listed in Table 2. The arithmetical mean height (Sa) is highest for parts manufactured with the brush, with a Sa of 6.16 µm. The lowest surface roughness with a Sa of 5.87 µm was determined for the parts manufactured with the polymer lip. The parts made with the HSS blade possessed a Sa of 5.98 µm. The maximum height difference, represented by the Sz value, shows a similar trend, with the lowest surface roughness measured for the parts produced with the lip. The differences between parts manufactured with the brush, lip, and HSS blade, however, are very small and not significant. The range between the lowest and highest Sa values is 0.29 µm, whereas for Sz it is 2.02 µm, which underlines the low deviations. No clear correlation can be derived from the surface roughness measurements. In general, Sz values are in the surface quality range determined by the VDI in a round robin test [40].

3.3.3. Dimensional accuracy

3.3.3.1. Rectangular specimens. The dimensional accuracy of the microstructure specimens with regard to measurement height (bottom, middle, top) and measurement direction (x- and y-direction) is shown in Fig. 10. Overall, all parts are smaller than the nominal dimension derived from the CAD data in the coating direction (x-direction). The smallest deviation from the CAD data in x-direction is observed when using the HSS blade. Deviations for the HSS blade in x-direction are in the range between 0.02 mm at the bottom and 0.05 mm at the top, whereas for the brush, the deviation lies in the range of 0.07 to 0.08 mm. The highest deviation in x-direction is observed for the lip, reaching from 0.08 to around 0.09 mm. Both the lip and the HSS blade show a

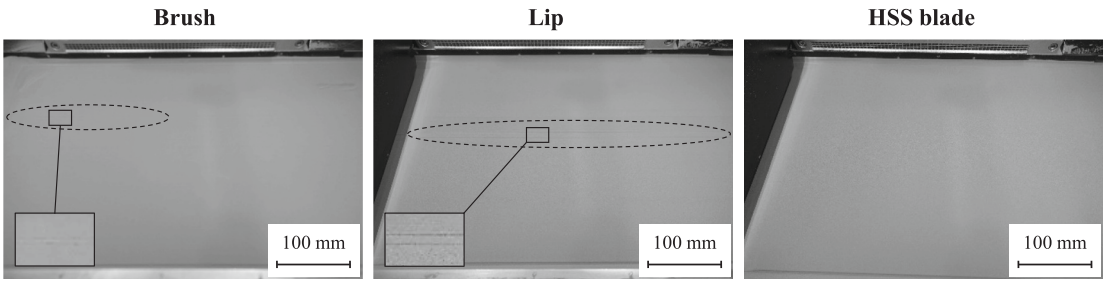

Fig. 8. Qualitative rating of homogeneity, with discontinuities (dashed lines) from using brush and lip marked and magnified (solid lines).

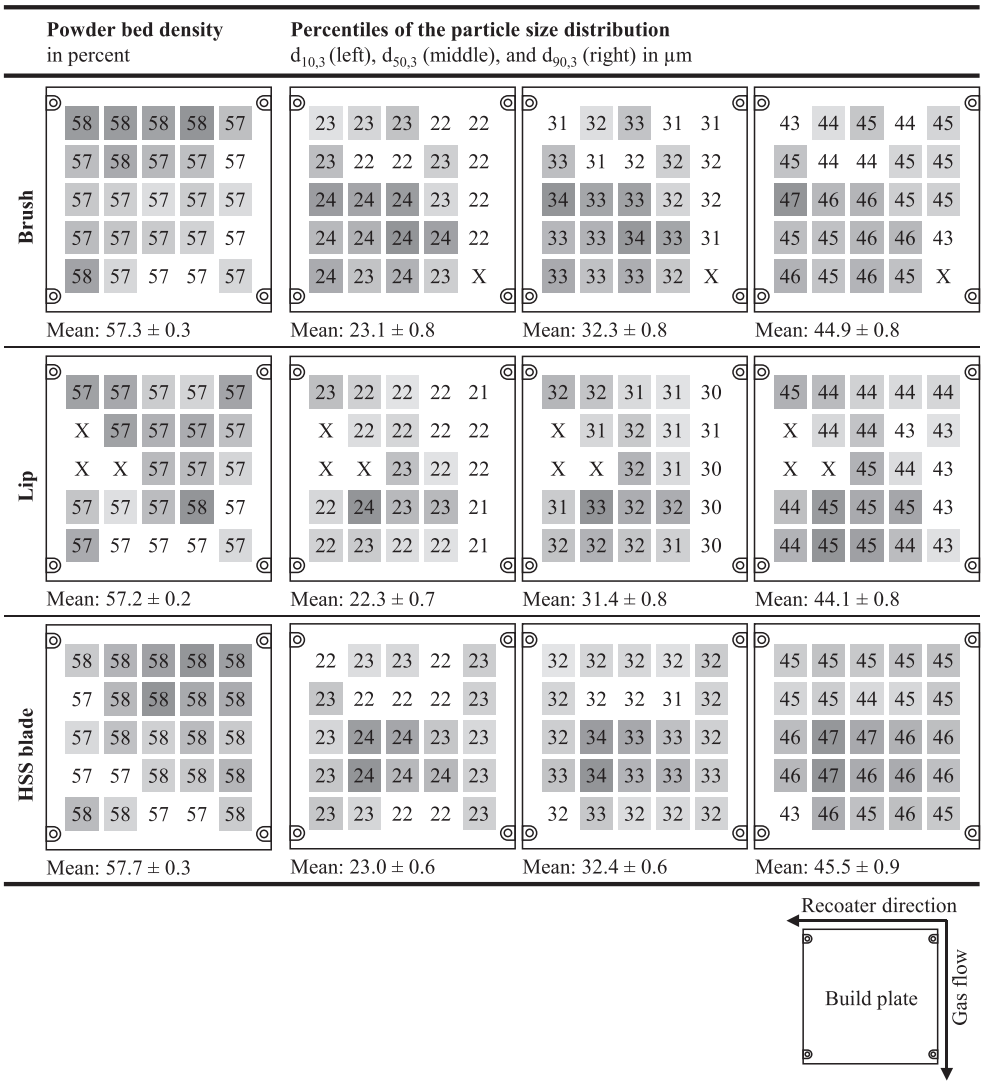

Fig. 9. Results of the powder bed density (PBD) and particle size distribution (PSD) analyses.

higher deviation at the top of the specimens in x-direction compared to the bottom. This tendency is also evident in the measurements taken along the direction of gas flow (y-axis). Here, the range of deviation for the HSS blade is from +0.01 to −0.05 mm. The amount of deviation resulting from the brush is highest at the top, at 0.06 mm. Deviation from the specimens manufactured with the lip are within a range of ±0.05 mm, regardless of the measurement height. Moreover, the standard deviation of the measurements is lowest when the HSS blade is used to create the specimens. In total, the brush and lip possess a lower dimensional accuracy than the HSS blade on simple geometries with sharp edges. Moreover, the deviation in y-direction is lower than in x-direction for the brush and lip.

3.3.3.2. Test artefact. The dimensional accuracy of the complex structures was determined from 3D scans of the test artefacts (c.f. Fig. 2 and Section 2.3). Geometrical deviations of holes perpendicular to the build direction, overhanging walls, and thin structures (cylindrical) were compared with the CAD geometry. The global best-fit method was chosen as the alignment method. Fig. 11 presents the geometrical deviations in pseudo color images (pci). All three test artefacts display a

Table 1
Evaluation of the buildability of thin walled specimens at 45 and 90° angles and part thicknesses of 0.2–0.8 mm.

Specimen			Spreading device		
Geometry	Thickness in mm	Build angle in °	Brush	Lip	HSS blade
Thin wall	0.2	90	Failed	Failed	Failed
	0.4	90	Failed	Failed	Failed
	0.6	90	**Built**	**Built**	Failed
	0.8	90	**Built**	**Built**	Failed
	0.2	45	Failed	Failed	Failed
	0.4	45	Failed	Failed	Failed
	0.6	45	**Built**	**Built**	Failed
	0.8	45	**Built**	**Built**	Failed
Rating	Failed: incomplete build, significant bending, delamination, lack of layer adhesion Built: complete build to 40 mm part height with no deviation; see Appendix				

Table 2
Mean values and standard deviations from the surface roughness measurements.

	Brush	Lip	HSS blade
Sa (in µm)	**6.16 ± 0.29**	**5.87 ± 0.48**	**5.98 ± 0.21**
Sz (in µm)	**65.03 ± 3.89**	**63.01 ± 6.39**	**64.18 ± 5.81**

large defect in the form of an edge on the downskin surfaces (60° and 75° overhang). Such edges occur with all recoaters at the tips of the drop-shaped cutouts. The maximum negative deviations (smaller than the CAD geometry) occur at the downskin edges and are between −0.27 and −0.29 mm for all spreading devices. The largest positive deviations are measured at the tips of the drop-shaped cutouts. A tendency towards lower, positive deviations was detected with the HSS blade (0.05 mm) in the small overhang surface. This compares with a deviation of 0.07 mm for the lip and the brush. Just like failing to build the thin wall specimens, the HSS blade damaged the smallest cylinder on the top of the test artefact that has a diameter of 1 mm. This supports the limitation of building thin structures with the HSS blade. Although the rectangular specimens display similar surface roughnesses, that of the surface of the brush part is noticeably higher and begins after the downskin defect. Besides this failure, the three test artefacts show similar characteristics, which is why the influence of the spreading device on the dimensional accuracy needs to be compared at specific spots in the 3D scan.

Fig. 12 shows the nominal deviations measured at ten points on the test artefact in dependency of the recoater used. The points are categorized into downskin, upskin, vertical and cylindrical walls as well as inside the cutouts, and positioned evenly over the test artefact. The majority of the points display a negative deviation of between −0.04 and −0.09 mm (excluding the downskin ridges). Comparing the deviation of the test artefacts made with different spreading devices, the maximum deviation is 0.02 mm. The largest positive deviation is observed inside a cutout of the part built with the HSS blade (0.14 mm, cf. Fig. 11, Point 9). This may be due to the lower scan quality inside the cutout resulting from shading caused by the optical measurement technique. Appendix A2 presents a pairwise comparison of the three spreading devices aligned to each other.

3.3.4. *Density and metallurgical structure*

The results of the density analysis are shown in Fig. 13 and reveal no significant differences in the impacts of the spreading devices. Absolute density is slightly above the common nominal values of between 8.17 [49] and 8.20 g/cm^3 [45]. This could be due to variation of the raw material or evaporation of lighter elements during PBF-LB/M processing. Porosity levels for all recoater variants are also very low, indicating generally high material densities and stable processes. These findings are supported by polished and etched cross-sections, as shown in Appendix (A3). Thus, the type of spreading device appears to have no effect either on the material density or on the general appearance of the metallurgical structure that can be measured by the applied methods.

3.3.5. *Tensile strength*

Despite the similarities in the density and porosity of the test pieces manufactured using different recoaters, the tensile strength shows some variation between build jobs, as shown in Fig. 14. The brush surpasses the other spreading devices with regard to the achievable UTS. Considering the standard deviation of all variants, the slight increase in the YS of the samples manufactured with the brush can be neglected; the values are at a comparable level. The mean fracture elongation values are identical. Samples manufactured using a silicone lip, however, show an increased variance in this respect. Additionally, stress-strain graphs of representative samples (Appendix A4, left) do not show any significant differences between the spreading devices. It should be noted that the samples investigated significantly surpass the results for YS and fracture elongation of the VDI round robin test and the lower limits of mechanical properties according to DIN EN 10302 [40] but are within the lower range of the nominal tensile strength given in DIN EN 10302. Nevertheless, all of the investigated properties are comparable with the median values given in the review by Hosseini and Popovich [39], which generally indicates good material fidelity and proves the usability of the samples.

3.3.6. *Criticality of abraded particles*

To investigate the criticality of particles abraded from the different spreading devices, test pieces were specifically contaminated with such

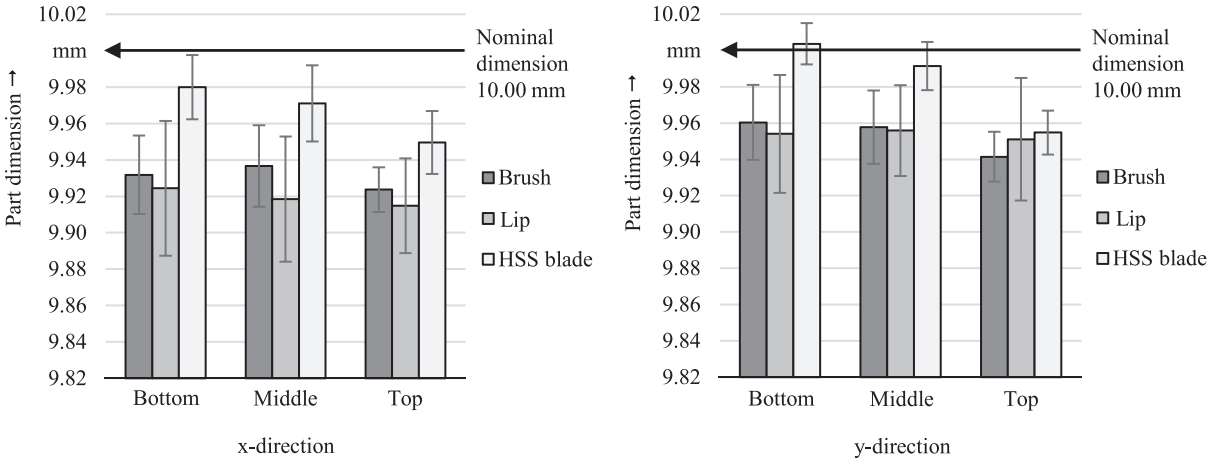

Fig. 10. Dimensional accuracy for the spreading devices (x-direction: coating direction; y-direction: gas flow).

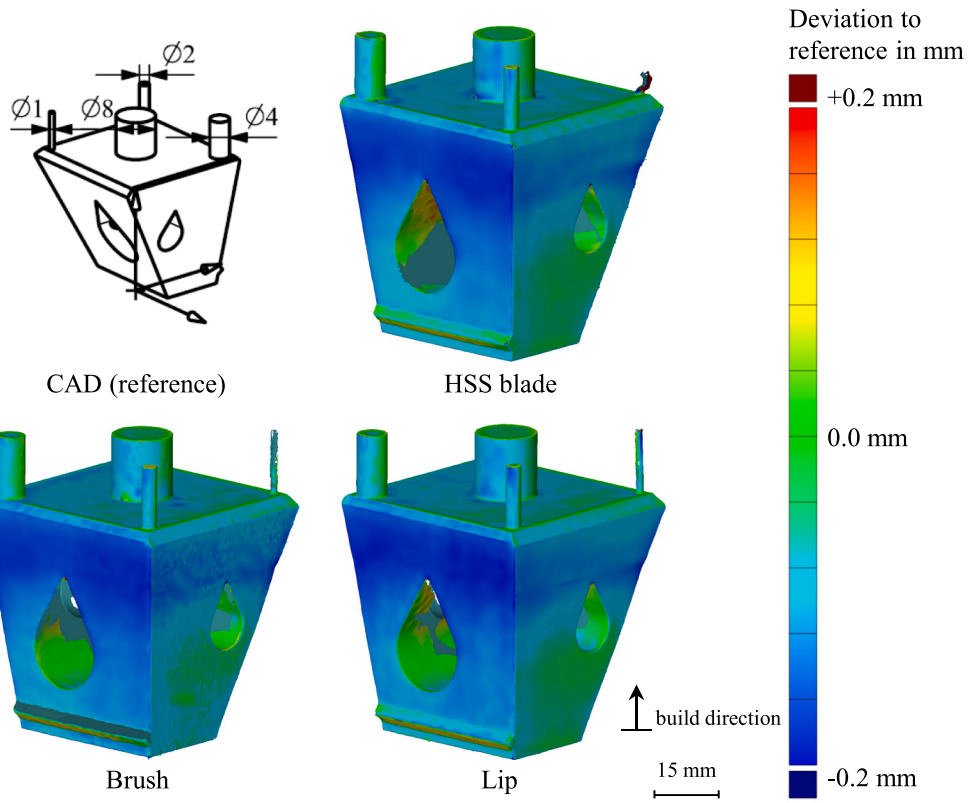

Fig. 11. Dimensional accuracy in 3D scans with pseudo color image. CAD data aligned to scanned parts manufactured using the different spreading devices.

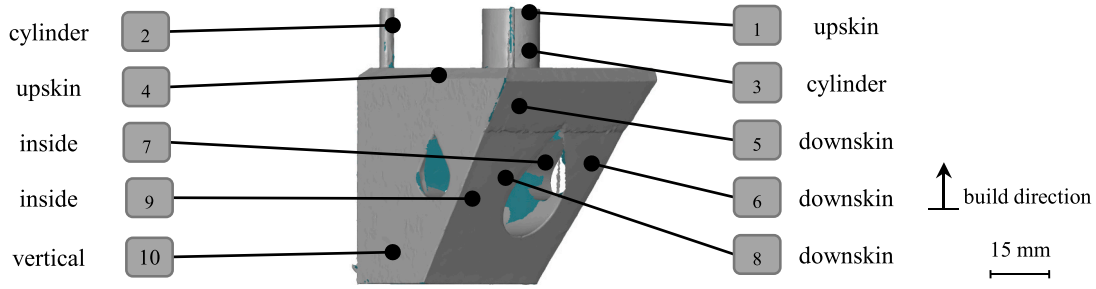

Points		1	2	3	4	5	6	7	8	9	10
Recoater medium	brush	-0.11	0.10	0.01	-0.08	-0.09	-0.16	-0.06	-0.05	0.07	-0.06
	lip	-0.09	0.09	-0.01	-0.07	-0.10	-0.18	0.08	-0.04	0.11	-0.05
	blade	-0.09	0.08	-0.01	-0.07	-0.09	-0.16	0.07	-0.04	0.14	-0.05

Fig. 12. Absolute deviation in mm of the test artefact. CAD data aligned to parts manufactured with the respective spreading devices.

particles, as described in Section 2.1. Fig. 15 presents images of the contaminants prior to, during, and after melting. The brush hair led to increased process radiation upon contact with the laser, indicating burning of the foreign material (Fig. 15d). After the layer had melted, a slightly elevated defect was observed on the solidified surface (Fig. 15j). Similar observations were also made for the HSS blade fragments. Although the process radiation did not increase as significantly, spots of afterglow were observed where some fragments were lying (Fig. 15f), which eventually formed elevated defects (Fig. 15l). Some blade fragments, however, were pushed into the powder bed as a result of the energy input (Fig. 15i). The latter was the predominant observation with the lip snippets (Fig. 15h). All foreign particles were pushed away by the melt pool dynamics and no defects were visible to the naked eye (Fig. 15k).

To detect internal flaws and to enable a comprehensive risk assessment, CT measurements were conducted in the region where the contaminants were located. Fig. 16 shows the measurements of the overall porosity and images of the pore distribution for the different contaminants, together with a reference sample. The porosity level in all specimens is very low, even below that of the specimens from build jobs 1–3 of ~0.005%, measured by visible light microscopy (VLM). The highest porosity of 0.0043% was observed for the sample contaminated with brush hair. The porosity of the other specimens is >50% lower and ranges from 0.0009% (reference) to 0.0014% (lip snippets) and on to 0.0020% (HSS blade fragments). It has to be considered that only features larger than ~36 μm in diameter were detected, which is sufficient

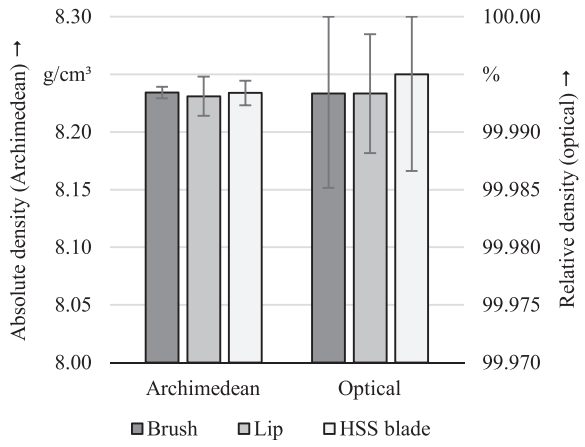

Fig. 13. Absolute and relative part density.

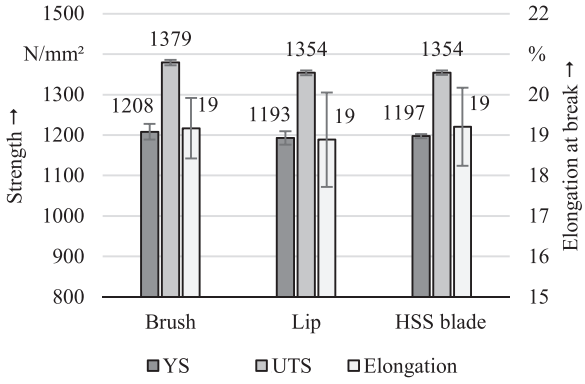

Fig. 14. Mechanical properties of specimens manufactured with the different spreading devices.

for the majority of applications, including the aerospace and medical industries. Smaller defects are omitted due to the CT's resolution. The pore distribution of the samples shows increased porosity at the part borders—regardless of the type of contamination. The majority of pores across all samples display diameters of ~75 μm. The sample contaminated with brush hair shows additional pores in its core, including some larger defects with diameters of >100 μm. Thus, contaminants do have negative influence on part porosity, especially at the core. The criticality, however, varies between lip snippets, HSS blade fragments, and brush hair. It can be concluded that the stronger the influence of the contaminant on the melting process (see: Fig. 15), the higher the level of porosity.

The tensile strength of contaminated samples was examined to determine the impact of the observed process quality and increase in porosity. Fig. 17 shows the results. Comparing the uncontaminated reference samples, which were built with a brush as the spreading device, with the respective uninterrupted samples (Fig. 14, Brush), the YS and UTS values were about 4.1% and 1.5% lower, respectively. The fracture elongation remained at about the same level. As all other factors remained constant, the process interruption of ~30 min, including the opening of the chamber door, is the most likely explanation for the slight material deterioration. Comparing the contaminated samples to the uncontaminated reference sample (Fig. 17), the YS and UTS levels are the same. With regard to the standard deviation of each variant, the influence of the contamination can be neglected. Only the fracture elongation displays some noteworthy differences. Samples contaminated with brush hair show slightly lower values, although their standard deviation is within the range of the reference sample. In contrast, HSS blade fragments lower the fracture elongation and significantly increase its standard deviation. Similarly, the stress-strain diagrams (see Appendix A4, right) and fracture surfaces, shown as examples in Appendix A5, do not reveal any differences in defect types or fracture dynamics.

Thus, the relation derived from the process observation (Fig. 15) and the porosity in the contamination zone (Fig. 16) is only partially transferable to the mechanical properties. While the fracture elongation is in line with previous findings, YS and UTS remain largely uneffaced by the particles abraded from the recoaters.

4. Discussion

The overall powder quality, expressed by the differences in PBD and PSD values across the build plate, was not significantly affected by the application of different spreading devices. Indeed, quite the contrary was observed, and measured values remained fairly stable across all build jobs. In general, the observed PBD values are in the same range as the findings of Ali et al. [34] and Jacob et al. [44], who investigated materials with densities similar to that of 2.4668. No pushing away of coarser particles along the coating direction and no differences in PSD and PBD [34] were observed in this investigation. Thus, Conjecture 1 can be rejected. The findings of Cao [28] and Le et al. [29], which suggested that better powder beds resulted from recoaters with planar surfaces, could not be confirmed in this study and Conjecture 2 can also be rejected. Additionally, the assumption that hard recoaters would yield higher PBDs due to higher forces being applied to the particles [33] was not reflected in this study and Conjecture 3 can be rejected, too. One noteworthy difference in the powder quality was revealed by top layer observation. As both soft recoaters were in contact with the thin wall specimens, they incurred a degree of damage and left grooves in the powder bed. The brush displayed better recovery from the damage than the lip, thanks to the flexibility of its hairs. However, both soft recoaters yielded successful build jobs despite the damage. The HSS blade was fully unable to effect successful manufacturing of the thin wall samples, but did not leave any grooves in the powder bed. The failure of the hard recoater is in line with the assumptions made by Diegel and Wohlers [13] and also Daňa et al. [31] and Conjecture 4 can be accepted.

The buildability investigation, which eventually led to the recoater contacts, revealed one of the major differences between the spreading devices. As the thin walls protruded upwards due to decreased heat dissipation into the powder bed, the HSS blade crashed and the job failed. In contrast, the elevated surfaces only damaged the soft recoaters, which partially recovered from the crash and eventually enabled successful build jobs. Thus, for complex parts or parameter studies that are prone to process variations, soft recoaters yield higher success rates, as predicted by Daňa et al. [31].

Dimensional deviations of below 100 μm in the rectangular specimens are on a par with the accuracy values found in the literature in the absence of any specific compensation strategies [50,51]. Increased distortion over the build height, which has been observed to similar extents with all spreading devices, is most likely responsible for the increase in geometry deviation from bottom to top [52]. Therefore, this effect cannot be attributed to the different recoaters. The predominant observations are the higher dimensional accuracy of the specimens in the y-direction and test pieces manufactured with the HSS blade. Regarding the former, Zhang et al. suggested that different cooling rates could be responsible for different deviations in x- and y-directions. However, this is unlikely to be the main influence in this study, due to the symmetricity of the samples and the scanning vector rotation. This is also supported by the test artefact, where the geometrical deviations of the parts manufactured with the HSS blade are among the smaller ones in the majority of categories. The increased dimensional accuracy of the HSS blade, especially with the cubic specimens, could be due to a smoother top layer resulting from the rigid and less adhesive surface of the blade, compared to the soft recoaters. Smoother layers increase the uniformity of the melt pool dimensions, which leads to increased

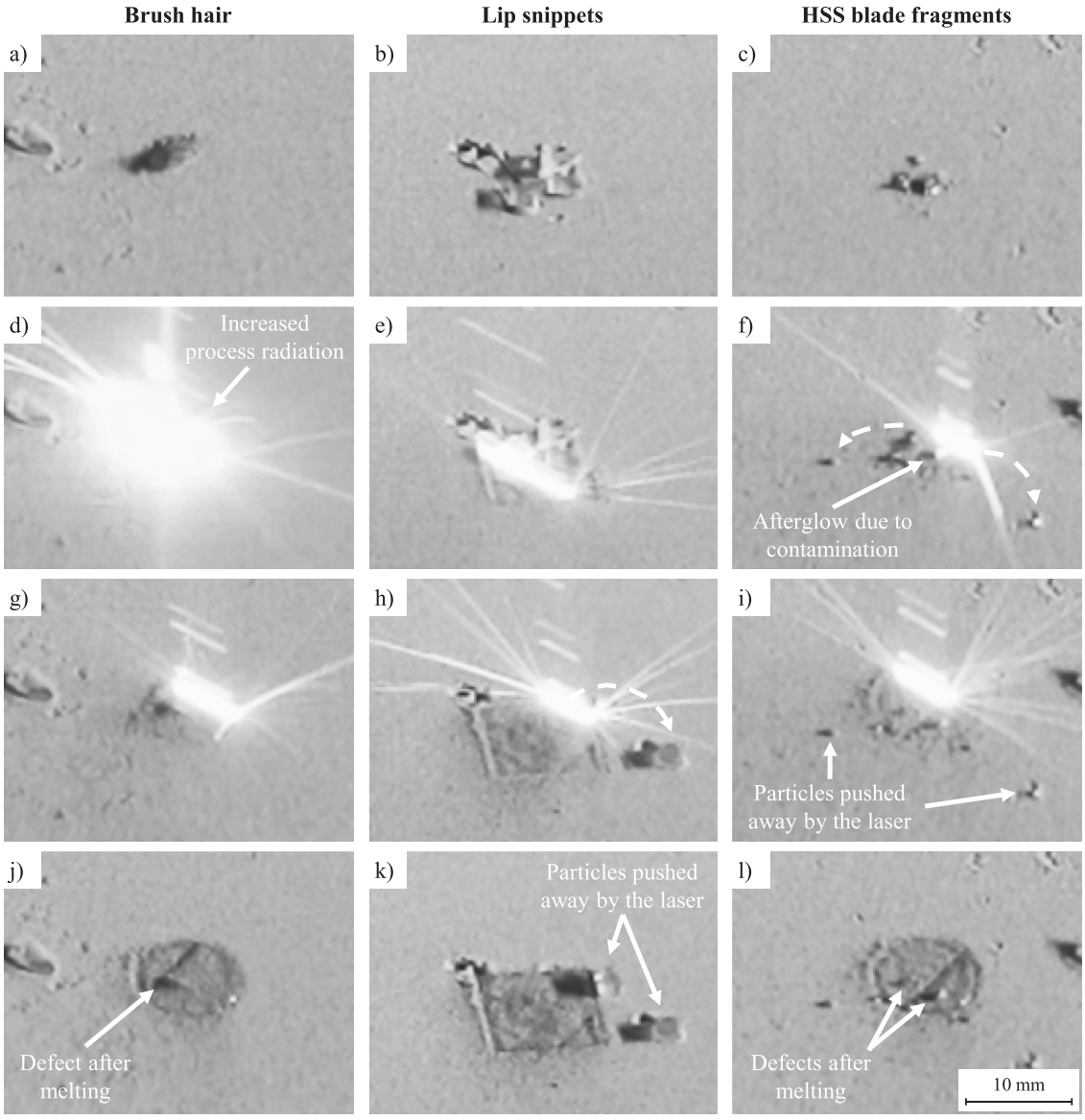

Fig. 15. Impact on the melting process of particles abraded from the spreading devices before (a–c), during (d–i), and after melting (j–l).

accuracy. To investigate this in greater detail, it is necessary to analyze the powder layer roughness in-situ during the build job or at least inside the machine, after the build job. The PBD measurement technique used and the resulting measurement values are insufficient to enable correlation of the PBD with the achievable accuracy. For intricate structures however, the two soft recoaters resulted in the finest features and test artefact, whereas the HSS blade failed in this respect.

All spreading devices yielded parts with similar surface qualities, material densities, and porosity levels. No significant differences were observed with regard to these three properties. The same applied to YS, UTS, and fracture elongation. This fits in with previous results, in that similar powder properties lead to parts with the same densities and, in turn, the same mechanical properties. This is also generally in line with the findings of Shamsdini et al. [33]. In contrast to the findings of the latter, however, fracture elongation was not reduced in this study when a brush was used as a powder spreading device. Furthermore, samples made using the brush that showed slightly increased UTS values are more likely to be positive outliers than specimens indicating any advantages of the brush. This is supported by the results for the test pieces contaminated with particles abraded from the spreading devices, where the uncontaminated reference samples manufactured using the brush are at the same UTS level as the other spreading devices.

Furthermore, the contaminated test pieces revealed the criticality of the brush hair and the HSS blade fragments. While the lip snippets were pushed away by the laser beam and yielded parts with porosity levels comparable to the reference sample, brush and blade particles affected the melting process. Although the melting point of carbon fiber is more than twice the liquidus temperature of alloy 2.4668 [49], due to the large surface of the contaminants (see: Fig. 6) and their high absorptivity of light in the facilitated wavelength range [53], it is likely that the fibers burnt and partially shaded the metal alloy surface from the laser. This insufficient energy input led to an increase in the amount of larger, non-spherical pores. The HSS blade fragments, in contrast, melted and created heat spots on the surface. As the fragments were larger than the 2.4668 metal particles, more energy was consumed during melting, which again led to insufficient energy input and increased porosity. As all tensile test pieces broke rather centered close to the interruption layer and no residue of the foreign particles was found during fractography, it is likely that the contaminants were either fully burnt or largely dissolved by the main material. The latter is a possible explanation for

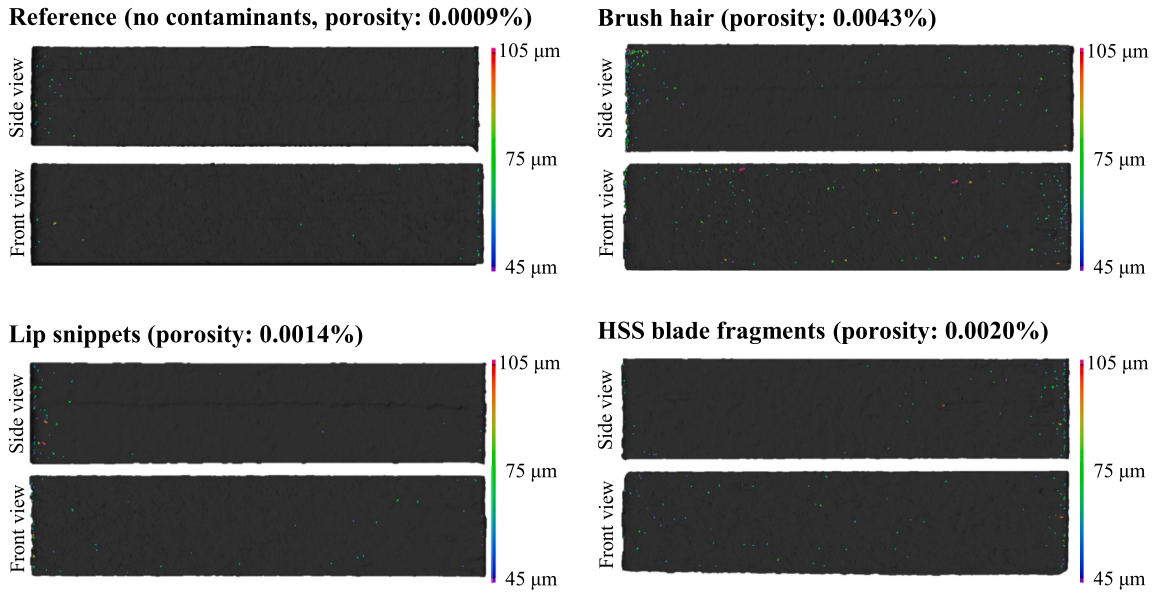

Fig. 16. CT scan images of the contaminated layer (± 1 mm), highlighting the pore distribution and total porosity in dependency of the contaminants (side view parallel to x-direction, front parallel to y-direction).

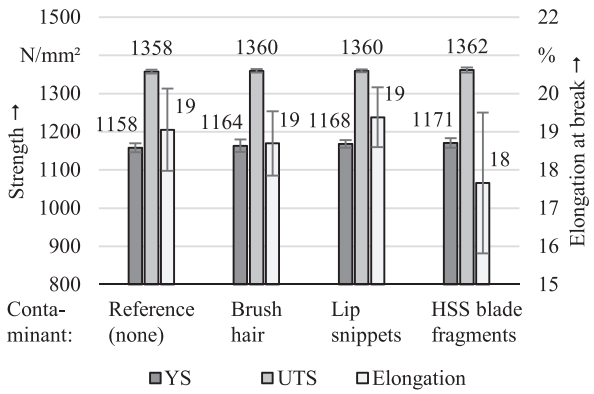

Fig. 17. Mechanical properties of contaminated specimens.

the slight decrease in fracture elongation. The main effect of the particles abraded from the spreading devices therefore appears to be that the laser beam and melting process were disrupted. However, apart from the decreased fracture elongation of some specimens contaminated with HSS blade fragments, the impact of increased porosity on the mechanical properties can be neglected. Additionally, the probability of blade fragments being abraded is smaller than that of brush hair being lost during recoating, which relativizes the risk to some extent. It can be concluded that smaller particles or smaller amounts of foreign particles than those found in this study probably have no significant negative effect on static tensile properties and Conjecture 5 can be rejected.

5. Compiling the selection guide

All the results were collected in a general evaluation scheme. The purpose of this is to present a guideline to enable users to select the most suitable spreading device for their applications, based on the presented findings. The three recoaters (brush, lip, and HSS blade) were rated on the basis of previously defined evaluation criteria. There was no weighting of the evaluation criteria, as this must be determined by the operators themselves, since it depends on the task at hand, for instance, whether it constitutes stable serial production or parameter development. A pairwise comparison of each evaluation criterion in accordance with VDI Guideline 2225 [37] is presented in A6. Ratings from the pairwise comparison presented in Table 3 were converted to give a representative overview of the impact of the spreading devices.

In terms of powder bed properties, all of the recoaters examined yield similar qualities. The buildability of the thin wall specimens was lowest for the HSS blade—independently of the wall thickness or angle. Applying a brush or lip allowed specimens to be built up to a minimum wall thickness of 0.6 mm. The highly flexible brush did not increase the buildability of specimens in this test set-up, unlike the polymer lip. Thus, the rigid HSS blade was found to be unsuitable for low wall thicknesses and parts of low stiffness. Moreover, as part protrusion cannot be compensated for, the HSS blade is best used in a well-tailored, stabilized process, possibly with application-specific parameters. The evaluation indicates that brushes and lips are better suited for building parts with low stiffness and for parameter development. In turn, overall dimensional accuracy is highest when the HSS blade is used in the manufacturing process, unbuildable filigree structures being the only exception. No distinction could be made regarding the achievable accuracy when using the brush or lip. Furthermore, all three spreading devices yield similar surface qualities, part densities, and mechanical properties. No significant differences were detected for these criteria. Regarding the criticality of abrasion particles from the recoaters, lip snippets appear to have an insignificant effect on porosity and

Table 3
Overall evaluation of spreading devices with regard to the respective criteria.

Evaluation criterion	Spreading device		
	Brush	Lip	HSS blade
Powder bed properties	0	0	0
Buildability	++	+	−−
Dimensional accuracy	−	−	++
Part density and microstructure	0	0	0
Tensile strength	0	0	0
Criticality of contaminants	−	+	−
Price	−	++	−
Rating	From disadvantageous (− −) over neutral (0) to advantageous (+ +). Derived from a pairwise comparison of spreading devices for each criterion (details shown in A6)		

mechanical properties. Recoater brush hair may lead to increased porosity but any impact on mechanical properties is negligible. If melted, HSS blade fragments may also lead to a minor increase in porosity and—far more critical—negatively affect fracture elongation. The price of the spreading devices was evaluated on the basis of quotations from the machine manufacturer with additional cost of mounting systems not being considered. The price of the brush is the highest of all the devices examined. A slightly reduced price is reported for the HSS blade. Both sides of the HSS blade can be used in the event that chips are lost due to contact with protruding parts. The lowest costs are associated with the polymer lip. The HSS blade is around nine times and the carbon fiber brush around 15 times more expensive than the polymer lip.

Overall, the results of the spreading device trials can be formulated as recommendations for PBF-LB/M machine operators as follows:

- If the PBF-LB/M process is well-tailored or mainly consists of bulky parts, the HSS blade should be considered as it has the best overall accuracy and powder bed stability. This is of particular benefit to serial production as it reduces downstream quality assurance and post-processing.
- To build complex parts of low stiffness, for example, due to high aspect ratios or low wall thickness, the soft recoaters possess beneficial properties compared to the stiffer HSS blade. Although the benchmarking based on thin-walled specimens produced no distinction between brush and lip, the lower stiffness and flexibility of the brush fibers could have even greater advantages for certain geometries.
- For research and development purposes, such as material qualification or geometry testing, that can result in elevated edges or balling, the brush or lip are recommended as recoaters, with the lip being the more economic option.
- If the sole purpose is to enable cost-effective PBF-LB/M production, the lip should be used. This is particularly the case where different parts are nested on the build plate for each machine job, as is commonly done by prototype service providers. Additionally, there is a lower risk of process interruption compared to the stiff HSS blade. But it is still possible for parts to be built with flaws, so additional quality assurance may be necessary in post-processing.
- Regulated industries such as aerospace are advised against using carbon brushes, since contamination testing was found to lead to an increased overall porosity with large pores. Brushes of metal fibers (e.g. 2.4668 fiber) could potentially mitigate the risk of contaminants while being less sensitive with regard to minor process variations.
- All experiments were conducted at a build plate temperature of 80 °C. Applying a high-temperature process at 500 °C or more to suppress crack growth [54] might limit the use of the polymer lip, so the more heat-resistant carbon brush or HSS blade might be preferable.

6. Conclusion and outlook

The main conclusion to be drawn from this study is that the similarities of the various spreading devises are greater than the differences. The HSS blade might have an edge over the soft recoaters for steady-state processes in terms of accuracy and stability. The brush and the lip, in turn, might be better suited for parameter development and design studies. Of the soft recoaters, the lip has the economic advantage, whereas the brush can be seen as an effective all-rounder. But in general, all three spreading devices resulted in highly stable processes and yielded powder bed and material properties on a par with—and at times surpassing—the reference values found in the literature. The selection guide based on the findings of this study is intended to help PBF-LB/M practitioners assess the minor differences between the spreading devices and serves as a basis by which to select the most suitable recoater for their application.

These findings could form the starting point for further investigation using different metal powders. Lightweight alloys in particular, such as aluminum or titanium alloys, could be affected differently by the spreading devices or their abrasion particles. Further studies could examine material properties, such as fatigue behavior, to better elaborate the differences between the recoaters. Moreover, the powder used in this investigation was relatively spherical, with a rather narrow PSD. Powders with less optimal properties and lower flowability might yield different results and could also be investigated in future studies. Once they are more established on the market, further investigations could also incorporate novel and contact-free designs [55–58], which will open up a whole new set of research questions.

CRediT authorship contribution statement

Max Horn: Conceptualization, Methodology, Investigation, Visualization, Writing – original draft. **Matthias Schmitt:** Conceptualization, Methodology, Investigation, Visualization, Writing – original draft. **Lukas Langer:** Investigation, Visualization, Writing – original draft. **Georg Schlick:** Writing – review & editing. **Christian Seidel:** Writing – review & editing, Supervision.

Declaration of competing interest

The authors declare that they have no conflicts of interest. The funders had no role in the design of the study; in the collection, analyses, or interpretation of data; in the writing of the manuscript, or in the decision to publish the results.

Data availability

Data will be made available on request.

Acknowledgements

The authors would like to express their sincere thanks to the German Research Foundation (DFG) and the Freistaat Bayern and Bavarian Ministry of Economic Affairs, Regional Development and Energy for providing the financial means for this research by funding the RE 1112/50-1 “Integrational lightweight design for gears by laser beam melting” and “MULTIMATERIALZENTRUM Augsburg” projects. Furthermore, the authors would like to thank Friederike Piossek, Norbert Zimmer, and Kurt Hartmann for their support in conducting the experiments. Open Access funding enabled and organized by Projekt DEAL.

Appendix A. Appendix

A.1. Documentation of a failed build job with an HSS blade due to recoater contact with thin wall specimens (left); deformation and delamination of thin wall specimens (0.2 and 0.4 mm thickness) using a brush (center) and lip (right) as spreading devices

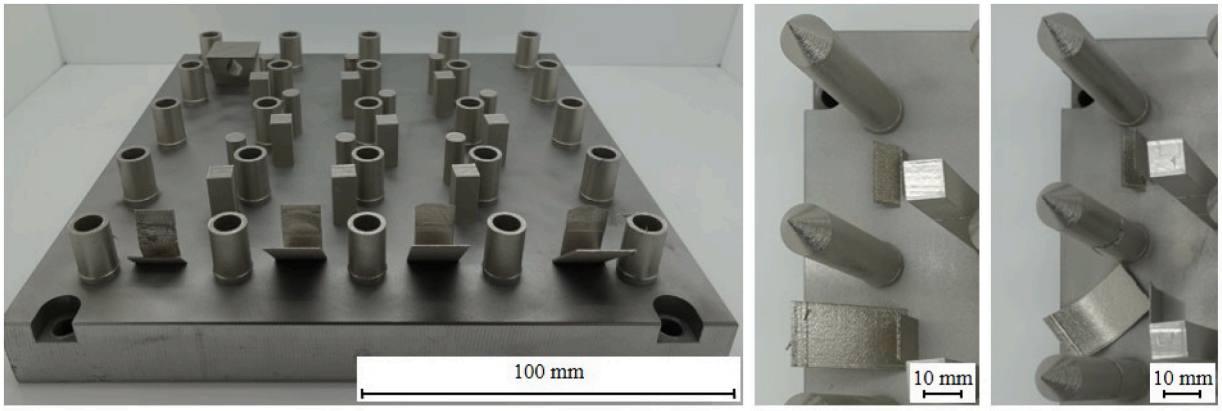

A.2. Dimensional accuracy of test artefacts. Pseudo color image (PCI) with pairwise comparison of the spreading devices. Comparison is aligned to reference by local best fit (vertical wall with hole)

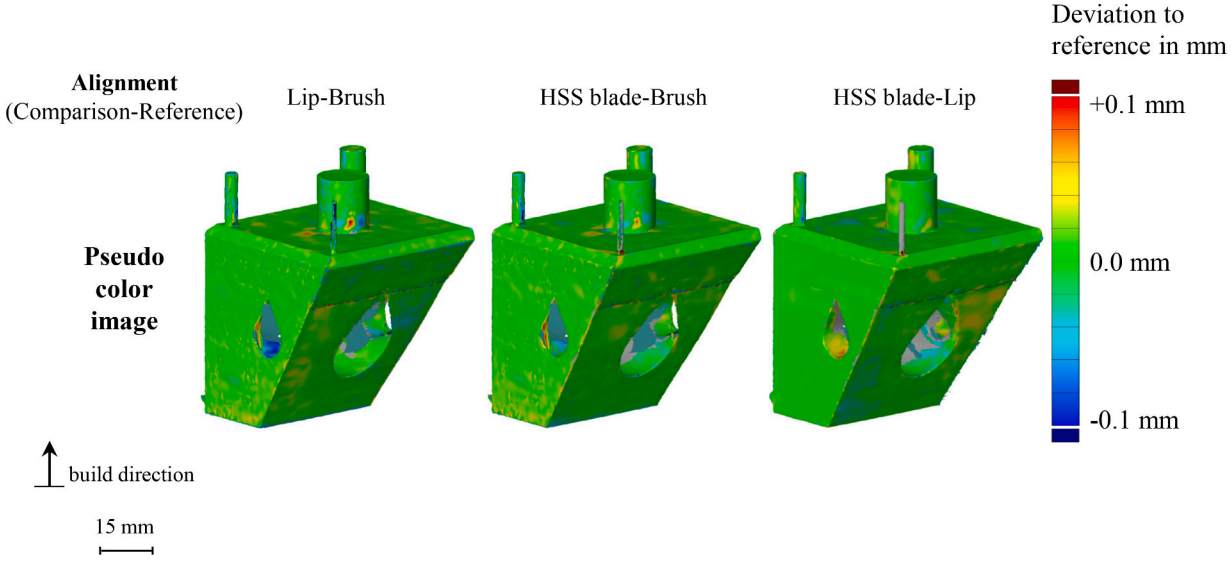

A.3. Micrographs of the samples with the lowest optical density, horizontal build plane (top row) and vertical build plane etched (bottom row)

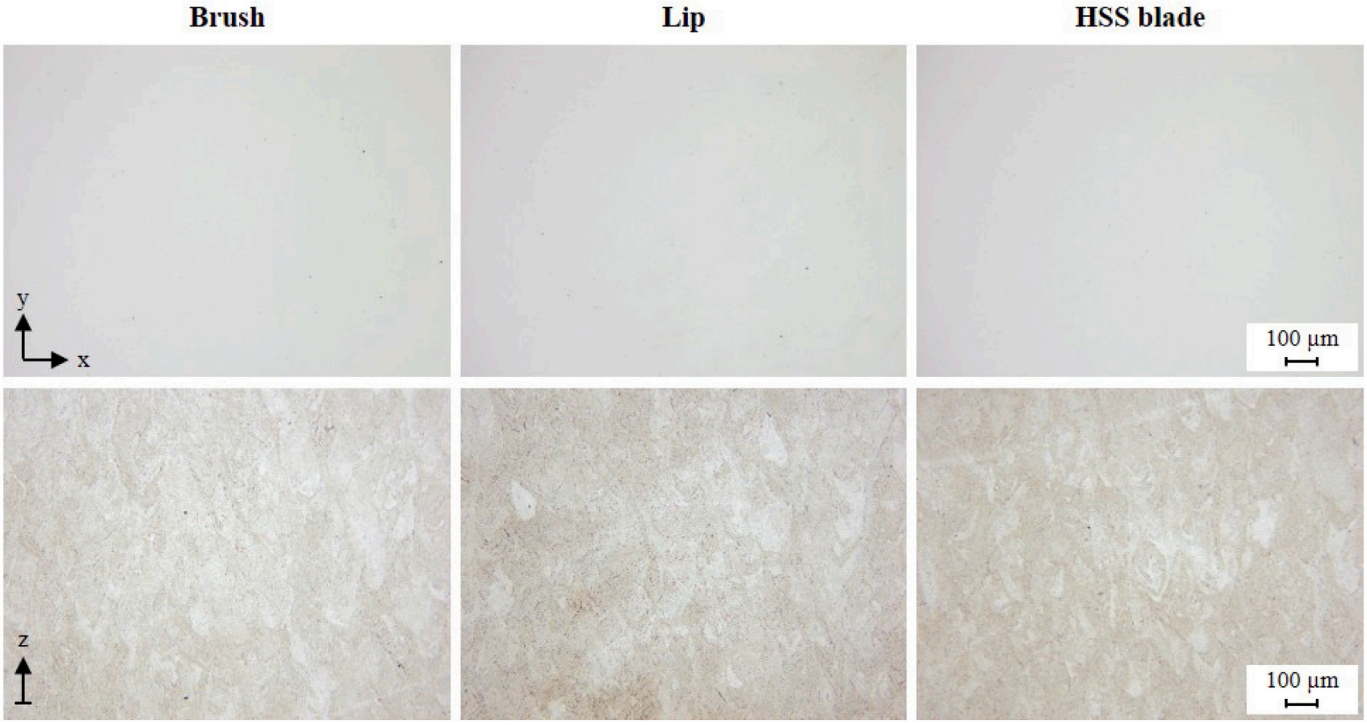

A.4. Stress-strain curves of median specimens for comparing spreading devices (left); influence of foreign particles abraded from recoaters (right)

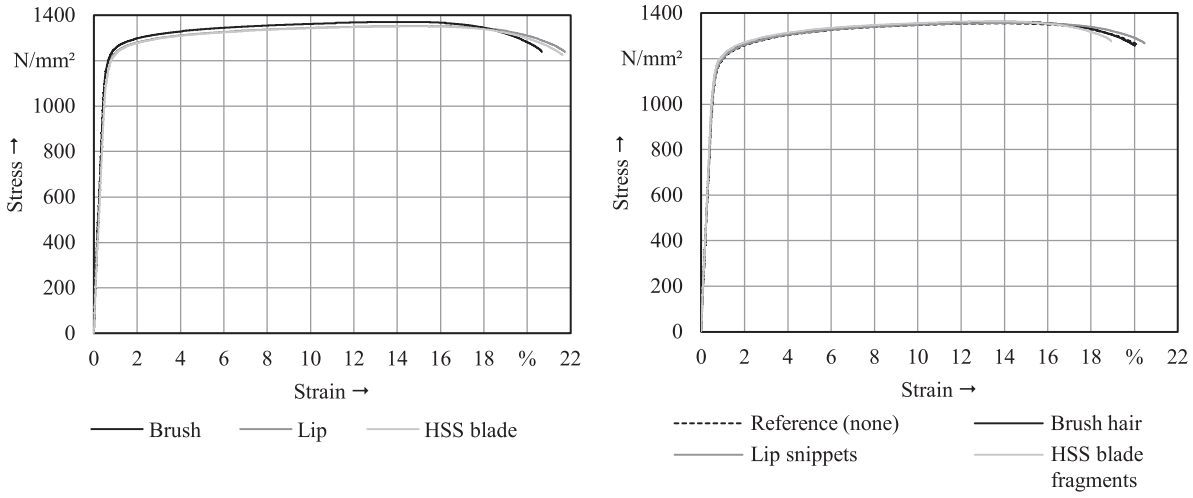

A.5. SEM images of representative specimens after tensile strength testing

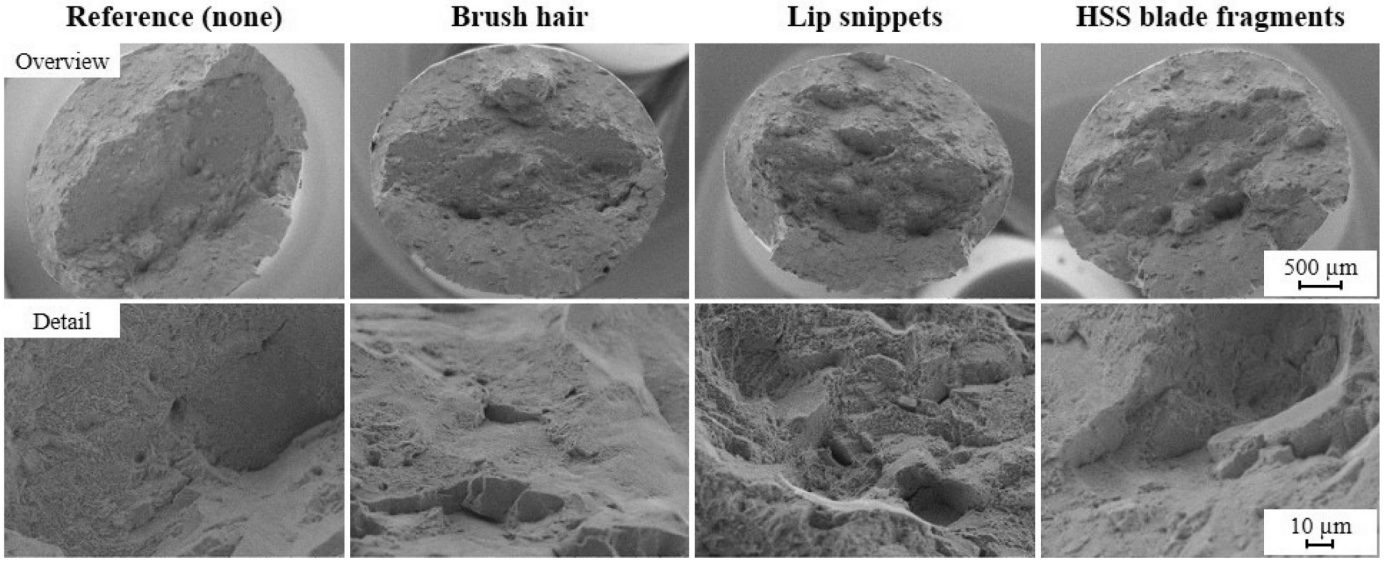

A.6. Pairwise comparison of recoater selection criteria

Powder Bed Properties	Lip	Brush	HSS Blade		Sum		Weight
Lip	x	1	1	→	2	→	0.333
Brush	1	x	1	→	2	→	0.333
HSS Blade	1	1	x	→	2	→	0.333
					6		1.000
					Sum		Sum

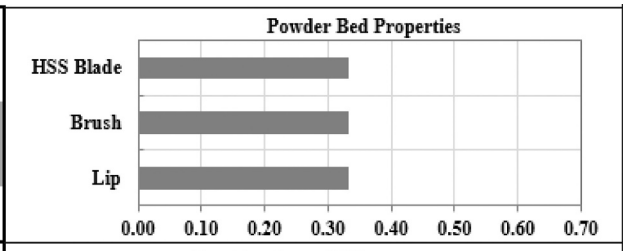

Part Density and Microstructure	Lip	Brush	HSS Blade		Sum		Weight
Lip	x	1	1	→	2	→	0.333
Brush	1	x	1	→	2	→	0.333
HSS Blade	1	1	x	→	2	→	0.333
					6		1.000
					Sum		Sum

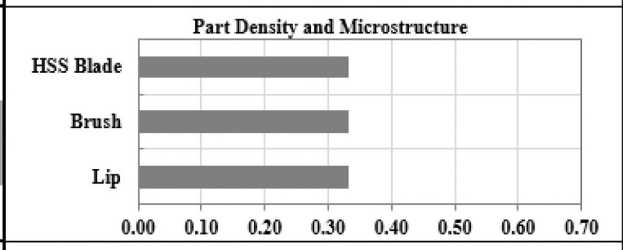

Dimensional Accuracy	Lip	Brush	HSS Blade		Sum		Weight
Lip	x	1	0	→	1	→	0.167
Brush	1	x	0	→	1	→	0.167
HSS Blade	2	2	x	→	4	→	0.667
					6		1.000
					Sum		Sum

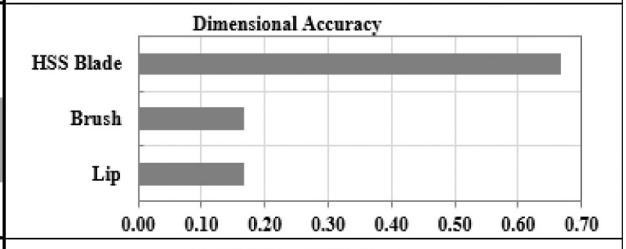

Buildability of Thin Parts	Lip	Brush	HSS Blade		Sum		Weight
Lip	x	0	2	→	2	→	0.333
Brush	2	x	2	→	4	→	0.667
HSS Blade	0	0	x	→	0	→	0.000
					6		1.000
					Sum		Sum

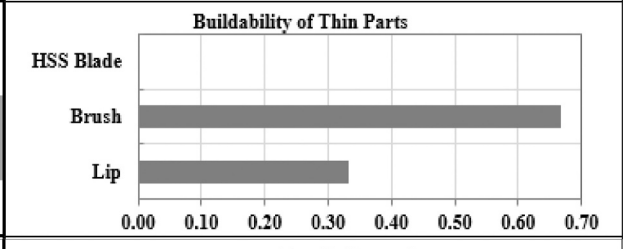

Tensile Strength	Lip	Brush	HSS Blade		Sum		Weight
Lip	x	1	1	→	2	→	0.333
Brush	1	x	1	→	2	→	0.333
HSS Blade	1	1	x	→	2	→	0.333
					6		1.000
					Sum		Sum

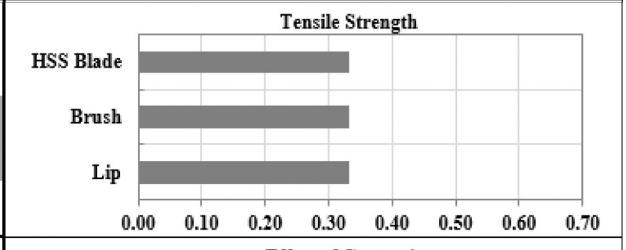

Effect of Contaminants	Lip	Brush	HSS Blade		Sum		Weight
Lip	x	2	2	→	4	→	0.667
Brush	0	x	1	→	1	→	0.167
HSS Blade	0	1	x	→	1	→	0.167
					6		1.000
					Sum		Sum

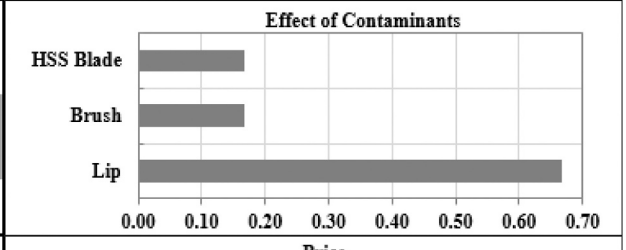

Price	Lip	Brush	HSS Blade		Sum		Weight
Lip	x	2	2	→	4	→	0.667
Brush	0	x	1	→	1	→	0.167
HSS Blade	0	1	x	→	1	→	0.167
					6		1.000
					Sum		Sum

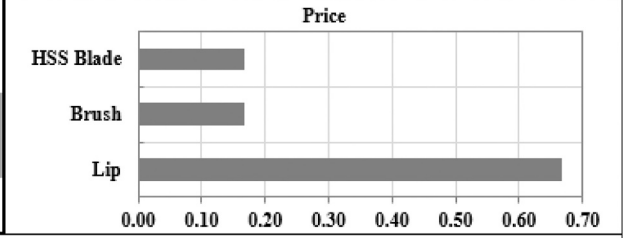

References

[1] M.F. Zaeh, Wirtschaftliche Fertigung mit Rapid-Technologien: Anwender-Leitfaden zur Auswahl geeigneter Verfahren, 1st ed., Hanser, München, 2013 [Online]. Available: http://www.hanser-elibrary.com/action/showBook?doi=10.3139/9783446439573.

[2] I. Gibson, D. Rosen, B. Stucker, Additive Manufacturing Technologies, Springer New York, New York, NY, 2015.

[3] O. Rehme, Cellular Design for Laser Freeform Fabrication, 1st ed., Cuvillier Verlag, Göttingen, 2010 [Online]. Available: https://ebookcentral.proquest.com/lib/kxp/detail.action?docID=5020518.

[4] M. van Elsen, Complexity of Selective Laser Melting: A New Optimisation Approach, Dissertation, KU Leuven, Leuven, Belgium, 2007.

[5] H. Krauss, Qualitätssicherung beim Laserstrahlschmelzen durch schichtweise thermografische In-Process-Überwachung, Dissertation,, Technical University Munich, Herbert Utz Verlag, Munich, Germany, 2016.

[6] Additive manufacturing processes, rapid manufacturing - Basics, definitions, processes, VDI 3405, The Association of German Engineers (VDI), Dec. 2014.

[7] S. Vock, B. Klöden, A. Kirchner, T. Weißgärber, B. Kieback, Powders for powder bed fusion: a review, Prog. Addit. Manuf. 4 (4) (2019) 383–397, https://doi.org/10.1007/s40964-019-00078-6.

[8] M.H. Sehhat, A. Mahdianikhotbesara, Powder spreading in laser-powder bed fusion process, Granul. Matter 23 (4) (2021), https://doi.org/10.1007/s10035-021-01162-x.

[9] DIN EN ISO/ASTM 52911–1:2020–05, Additive Fertigung_- Konstruktion_- Teil_1: Laserbasierte Pulverbettfusion von Metallen (ISO/ASTM 52911–1:2019); Deutsche Fassung EN_ISO/ASTM 52911–1:2019, Berlin.

[10] MSFC-SPEC-3717: Specification for Control and Qualification of Laser Powder Bed Fusion Metallurgical Processes, MSFC-SPEC-3717, NASA Standard, Oct. 2017 [Online]. Available: https://standards.nasa.gov/standard/msfc/msfc-spec-3717.

[11] DIN SPEC 17071:2019–12, Additive Fertigung_- Anforderungen an qualitätsgesicherte Prozesse für additive Fertigungszentren; Text in Deutsch und Englisch, Berlin.

[12] H. Chen, Q. Wei, Y. Zhang, F. Chen, Y. Shi, W. Yan, Powder-spreading mechanisms in powder-bed-based additive manufacturing: experiments and computational modeling, Acta Mater. 179 (2019) 158–171, https://doi.org/10.1016/j.actamat.2019.08.030.

[13] O. Diegel, T. Wohlers, From silicone and rubber to steel and ceramic: the weird and wonderful world of wipers, Metal Add. Manufact. 5 (4) (2019) 137–139 [Online]. Available: https://www.metal-am.com/wp-content/uploads/sites/4/2019/12/MAGAZINE-Metal-AM-Winter-2019-double-page.pdf.

[14] P.S. Desai, C.F. Higgs, Spreading process maps for powder-bed additive manufacturing derived from physics model-based machine learning, Metals 9 (11) (2019) 1176, https://doi.org/10.3390/met9111176.

[15] E.J.R. Parteli, T. Pöschel, Particle-based simulation of powder application in additive manufacturing, Powder Technol. 288 (2016) 96–102, https://doi.org/10.1016/j.powtec.2015.10.035.

[16] S. Haeri, Y. Wang, O. Ghita, J. Sun, Discrete element simulation and experimental study of powder spreading process in additive manufacturing, Powder Technol. 306 (4) (2017) 45–54, https://doi.org/10.1016/j.powtec.2016.11.002.

[17] J. Zhang, Y. Tan, T. Bao, Y. Xu, X. Xiao, S. Jiang, Discrete element simulation of the effect of roller-spreading parameters on powder-bed density in additive manufacturing, Materials (Basel, Switzerland) vol. 13 (10) (2020), https://doi.org/10.3390/ma13102285.

[18] B. Nagarajan, Z. Hu, X. Song, W. Zhai, J. Wei, Development of micro selective laser melting: the state of the art and future perspectives, Engineering 5 (4) (2019) 702–720, https://doi.org/10.1016/j.eng.2019.07.002.

[19] S. Weber, J. Montero, M. Bleckmann, K. Paetzold, Support-free metal additive manufacturing: a structured review on the state of the art in academia and industry, Proc. Des. Soc. 1 (2021) 2811–2820, https://doi.org/10.1017/pds.2021.542.

[20] A. Khorasani, I. Gibson, J.K. Veetil, A.H. Ghasemi, A review of technological improvements in laser-based powder bed fusion of metal printers, Int. J. Adv. Manuf. Technol. 108 (1–2) (2020) 191–209, https://doi.org/10.1007/s00170-020-05361-3.

[21] J. Zhang, Y. Tan, X. Xiao, S. Jiang, Comparison of roller-spreading and blade-spreading processes in powder-bed additive manufacturing by DEM simulations, Particuology 66 (2) (2022) 48–58, https://doi.org/10.1016/j.partic.2021.07.005.

[22] Z. Xiang, M. Zhang, R. Yan, Q. Yin, K. Zhang, Powder-spreading dynamics and packing quality improvement for laser powder bed fusion additive manufacturing, Powder Technol. 389 (2021) 278–291, https://doi.org/10.1016/j.powtec.2021.05.036.

[23] C. Meier, R. Weissbach, J. Weinberg, W.A. Wall, A.J. Hart, Critical influences of particle size and adhesion on the powder layer uniformity in metal additive manufacturing, J. Mater. Process. Technol. 266 (2019) 484–501, https://doi.org/10.1016/j.jmatprotec.2018.10.037.

[24] M. Mitterlehner, H. Danninger, C. Gierl-Mayer, J. Frank, W. Tomischko, H. Gschiel, Novel testing device and routine to characterise the spreadability of powders for powder bed fusion processes – a problem-oriented approach, Powder Metall. 165 (3) (2022) 1–17, https://doi.org/10.1080/00325899.2021.2023414.

[25] M. Mitterlehner, H. Danninger, C. Gierl-Mayer, M. Fürst, H. Gschiel, Spreading behaviour and packing density of the powder bed in L-PBF as a function of spreading strategy and velocity, in: Proceedings of the Euro PM2020 Virtual Congress & Exhibition, 2020.

[26] Z. Snow, R. Martukanitz, S. Joshi, On the development of powder spreadability metrics and feedstock requirements for powder bed fusion additive manufacturing, Addit. Manuf. 28 (5) (2019) 78–86, https://doi.org/10.1016/j.addma.2019.04.017.

[27] L. Wang, A. Yu, E. Li, H. Shen, Z. Zhou, Effects of spreader geometry on powder spreading process in powder bed additive manufacturing, Powder Technol. 384 (2021) 211–222, https://doi.org/10.1016/j.powtec.2021.02.022.

[28] L. Cao, Study on the numerical simulation of laying powder for the selective laser melting process, Int. J. Adv. Manuf. Technol. 105 (5–6) (2019) 2253–2269, https://doi.org/10.1007/s00170-019-04440-4.

[29] T.-P. Le, X. Wang, K.P. Davidson, J.E. Fronda, M. Seita, Experimental analysis of powder layer quality as a function of feedstock and recoating strategies, Addit. Manuf. 39 (8) (2021) 101890, https://doi.org/10.1016/J.ADDMA.2021.101890.

[30] S. Haeri, Optimisation of blade type spreaders for powder bed preparation in additive manufacturing using DEM simulations, Powder Technol. 321 (2017) 94–104, https://doi.org/10.1016/j.powtec.2017.08.011.

[31] M. Daňa, I. Zetková, P. Hanzl, The influence of a ceramic Recoater blade on 3D printing using direct metal laser sintering, Manufact. Technol. 19 (1) (2019) 23–28, https://doi.org/10.21062/ujep/239.2019/a/1213-2489/MT/19/1/23.

[32] M.Y. Shaheen, A.R. Thornton, S. Luding, T. Weinhart, The influence of material and process parameters on powder spreading in additive manufacturing, Powder Technol. 383 (2021) 564–583, https://doi.org/10.1016/j.powtec.2021.01.058.

[33] S. Shamsdini, M.H. Ghoncheh, M. Mohammadi, Effect of recoater-blade type on the mechanical properties and microstructure of additively manufactured maraging steels, Mater. Sci. Eng. A 812 (4) (2021) 141104, https://doi.org/10.1016/j.msea.2021.141104.

[34] U. Ali, et al., On the measurement of relative powder-bed compaction density in powder-bed additive manufacturing processes, Mater. Des. 155 (11) (2018) 495–501, https://doi.org/10.1016/j.matdes.2018.06.030.

[35] M.S. Palm, M. Horn, A. Bachmann, G. Schlick, M.F. Zaeh, G. Reinhart, Influence of contaminants on part quality during laser-based powder bed fusion of nickel base alloys, Proc. CIRP 94 (3) (2020) 233–238, https://doi.org/10.1016/j.procir.2020.09.044.

[36] Electro Optical Systems (EOS) GmbH, Use-cases of different recoater configurations. [Online]. Available: https://www.eos.info/en/blog-articles/recoater-configurations-for-dmls (accessed: May 4 2022.266Z).

[37] Design engineering methodics - Engineering design at optimum cost - Valuation of costs, VDI 2225 Part 3, The Association of German Engineers (VDI), Nov. 1998.

[38] T.T. Wohlers, I. Campbell, O. Diegel, R. Huff, J. Kowen, Wohlers Report 2022: 3D Printing and Additive Manufacturing Global State of the Industry, Wohlers Associates, Fort Collins, Colorado, 2022.

[39] E. Hosseini, V.A. Popovich, A review of mechanical properties of additively manufactured Inconel 718, Addit. Manuf. 30 (10) (2019) 100877, https://doi.org/10.1016/j.addma.2019.100877.

[40] Additive manufacturing processes - Laser beam melting of metallic parts - Material data sheet nickel alloy material number 2.4668, VDI 3405 Part 2.2, The Association of German Engineers (VDI), Jul. 2017.

[41] Nickel Alloy, *Corrosion and Heat-Resistant, Bars, Forgings, and Rings 52.5Ni - 19Cr - 3.0Mo - 5.1Cb (Nb) - 0.90Ti - 0.50AI - 18Fe Consumable Electrode or Vacuum Induction Melted 1775 °F (968 °C) Solution Heat Treated, Precipitation-Hardenable,* AMS5662N, SAE Internatinal, Jun. 2016.

[42] B. Liu, R. Wildman, C. Tuck, I. Ashcroft, R. Hague, Investigation the effect of particle size distribution on processing parameters optimisation in selective laser melting process, in: Proceedings of the International Solid Freeform Fabrication Symposium, 2011.

[43] M. Lutter-Günther, M. Horn, C. Seidel, G. Reinhart, Einfluss der Korngrößenverteilung auf Fließfähigkeit und Bauteilqualität beim Laserstrahlschmelzen, in: M. Kynast, M. Eichmann, G. Witt (Eds.), Hanser eLibrary, Rapid.Tech - International Trade Show & Conference for Additive Manufacturing: Proceedings of the 14th Rapid.Tech Conference, Erfurt, Germany, 20–22 June 2017, Hanser, München, 2017, pp. 297–311.

[44] G. Jacob, A. Donmez, J. Slotwinski, S. Moylan, Measurement of powder bed density in powder bed fusion additive manufacturing processes, Meas. Sci. Technol. 27 (11) (2016) 115601, https://doi.org/10.1088/0957-0233/27/11/115601.

[45] A.S. Hakeem, et al., Comparative evaluation of thermal and mechanical properties of nickel alloy 718 prepared using selective laser melting, spark plasma sintering, and casting methods, J. Mater. Res. Technol. 12 (2021) 870–881, https://doi.org/10.1016/j.jmrt.2021.03.043.

[46] *DIN EN ISO 25178-1:2016–12,* Geometrische Produktspezifikation_(GPS)_- Oberflächenbeschaffenheit: Flächenhaft_- Teil_1: Angabe von Oberflächenbeschaffenheit (ISO_25178–1:2016); Deutsche Fassung EN_ISO_25178–1:*2016*, Berlin.

[47] DIN EN ISO 10360-1:2003–07, Geometrische Produktspezifikation (GPS)_- Annahmeprüfung und Bestätigungsprüfung für Koordinatenmessgeräte (KMG)_- Teil_1: Begriffe (ISO_10360–1:2000_+ Corr_1:2002) (enthält Berichtigung_AC: 2002); Deutsche Fassung EN_ISO_10360–1:2000_+ AC:2002, Berlin.

[48] *DIN EN ISO 6892-1:2020–06,* Metallische Werkstoffe_- Zugversuch_- Teil_1: Prüfverfahren bei Raumtemperatur (ISO_6892–1:2019); Deutsche Fassung EN_ISO_6892–1:2019, Berlin.

[49] H.P. Wang, C.H. Zheng, P.F. Zou, S.J. Yang, L. Hu, B. Wei, Density determination and simulation of Inconel 718 alloy at normal and metastable liquid states, J. Mater. Sci. Technol. 34 (3) (2018) 436–439, https://doi.org/10.1016/j.jmst.2017.10.014.

[50] L. Zhang, S. Zhang, H. Zhu, Z. Hu, G. Wang, X. Zeng, Horizontal dimensional accuracy prediction of selective laser melting, Mater. Des. 160 (2018) 9–20, https://doi.org/10.1016/j.matdes.2018.08.059.

[51] S. Gruber, et al., Comparison of dimensional accuracy and tolerances of powder bed based and nozzle based additive manufacturing processes, J. Laser Appl. 32 (3) (2020) 32016, https://doi.org/10.2351/7.0000115.
[52] S. Afazov, W.A.D. Denmark, B. Lazaro Toralles, A. Holloway, A. Yaghi, Distortion prediction and compensation in selective laser melting, Addit. Manuf. 17 (12) (2017) 15–22, https://doi.org/10.1016/j.addma.2017.07.005.
[53] C.D. Boley, A.M. Rubenchik, Modeling of laser interactions with composite materials, Appl. Opt. 52 (14) (2013) 3329–3337, https://doi.org/10.1364/AO.52.003329.
[54] A.V. Mueller, et al., Additive manufacturing of pure tungsten by means of selective laser beam melting with substrate preheating temperatures up to 1000 ∘C, Nuclear Mater. Energy 19 (9–10) (2019) 184–188, https://doi.org/10.1016/j.nme.2019.02.034.
[55] A. Bedoret, M. Hick, and K. Eckes, "Device and method for creating a particle structure," BE1024613B1, Belgium.
[56] J. Foerster, M. Michatz, C. Anstaett, C. Seidel, J. Schilp, Aspects of developing a powder application module based on electrophotography for additive powder bed based processes, SSRN J. (2020), https://doi.org/10.2139/ssrn.3724131.
[57] J. Foerster, et al., Electrostatic powder attraction for the development of a novel recoating system for metal powder bed-based additive manufacturing, J. Electrost. 115 (2022) 103641, https://doi.org/10.1016/j.elstat.2021.103641.
[58] B. Buller, T. Lappas, E. Milshtein, R. Mendelsberg, K. Symeonidis, and A. R. Lappen, "Skillful Three-Dimensional Printing," US2017/0165754A1, USA.